Wireless Identification and Sensing using Surface Acoustic Wave Devices

by

Leo P Schuler

A thesis
presented to the University of Canterbury
in fulfilment of the
thesis requirement for the degree of
Masters
in
Engineering

Christchurch, New Zealand, 2003

Acknowledgements

I would like to thank Dr. Maan Alkaisi, Dr. Richard Blaikie, and Warren Meade for their direction, assistance, and guidance. I am particularly grateful to Dr. Paul Muralt of EPFL, for his recommendations and suggestions in the area of sputtering, which have been invaluable for the project.

I also wish to thank Dr. James Conway of Stanford Nanofabrication Facility, Professor Wei Gao of University of Auckland and Dr. Andreas Markwitz of Institute of Geological and Nuclear Sciences in Lower Hutt, for their help towards my research.

I am grateful to Helen Devereux, Gary Turner, Malcom Gordon and the other lab personnel for their help and support.

I am indebted to my thesis committee, Dr. Gerard Rowe of Auckland University and Dr. Maan Alkaisi who kindly agreed to be examiners.

Special thanks should be given to my student colleagues who helped me in many ways. Finally, words alone cannot express the thanks I owe to Helen, my wife, for her encouragement and assistance.

I wish to thank my employer both for financial and logistical support and the Foundation for Science and Research (FRST) for awarding me a Bright Future Scholarship.

Abstract

Wireless Surface Acoustic Wave (SAW) devices were fabricated and tested using planar Lithium Niobate ($LiNbO_3$) as substrate. The working frequencies were in the 180 MHz and 360 MHz range. Using a network analyser, the devices were interrogated with a wireless range of more than 2 metres. Trials with Electron Beam Lithography (EBL) to fabricate SAW devices working in the 2450 MHz with a calculated feature size of 350 nm are discussed. Charging problems became evident as $LiNbO_3$ is a strong piezoelectric and pyroelectric material. Various attempts were undertaken to neutralise the charging problems.

Further investigation revealed that sputtered Zinc Oxide (ZnO) is a suitable material for attaching SAW devices on irregularly shaped material. DC sputtering was used and several parameters have been optimised to achieve the desired piezoelectric effect.

ZnO was sputtered using a magnetron sputtering system with a 75 mm Zn target and a DC sputter power of 250 Watts. Several trials were performed and an optimised material has been prepared under the following conditions: 9 sccm of Oxygen and 6 sccm of Argon were introduced during the process which resulted in a process pressure of 1.2×10^{-2} mbar. The coatings have been characterised using Rutherford Backscattering, X-ray diffraction, SEM imaging, and Atomic force microscopy. SAW devices were fabricated and tested on 600 nm thick sputtered ZnO on a Si substrate with a working frequency of 430 MHz. The phase velocity has been calculated as 4300m/s.

Non-planar samples have been coated with 500 nm of sputtered ZnO and SAW structures have been fabricated on using EBL. The design frequency is 2450 MHz, with a calculated feature size of 1 μm. The surface roughness however prevented a successful lift-off. AFM imaging confirmed a surface roughness in the order of 20 nm. Ways to improve manufacturability on these samples have been identified.

Table of Contents

List of figures

List of tables

Chapter 1
Introduction

This project was initiated by an industry partner, who manufactures machines which have expensive wearing parts, up to 2000 per machine. Throughout this thesis, these parts will be called "rods". If one of these rods fail, considerable quantities of defective product would be produced, incurring high losses and down time. As the rods are costly to replace, the owner of the machines is interested to get the maximum service life out of the parts. In addition, these rods can become misaligned or blunt, leading to an inferior product. Therefore, a way was sought to run a "health check" on the rods. Preliminary trials showed, that by measuring instantaneous strain, several critical values can be inferred: Misalignment, rod not being sharp or no material flow. The rods are very small; therefore it is not practicable to use off-the-shelf strain gauges due to size, weight, and cost. The rods are also subject to rapid motion and are not easily accessible; therefore a wireless solution is preferred.

Table 1: Possible approaches for measuring strain on mechanical parts (as of September 2001).

Technology	**Resistor Strain gauge**	**Semiconductor Strain gauge**	**SAW device** as strain gauge	**FBAR** device as strain gauge
Details	Resistor strain gauges are commonly used parts. A strain gauge amplifier is needed to convert the small signals.	Semiconductor Strain gauges are very small, fragile, and quite hard to work with. A strain gauge amplifier is needed to convert the small signals.	SAW (Surface Acoustic Wave) device would sense strain and possible temperature in area of interest	FBAR (Film Bulk Acoustic Resonator) can be used similarly to SAW devices
Advantages	Good accuracy and repeatability of measurements.	Smaller than Resistor Strain gauges. Can be incorporated in individual rods.	Wireless Data exchange. Powered via radio waves. Well-established technology. Low production/ assembly costs.	Even smaller than SAW devices.
Disadvantages	Needs power supply. High price. High labour component. Difficult to place on small mechanical parts due to size.	Needs power supply. High price. High labour component.	Not yet on the market.	Immature technology. No possibility to develop locally.

Extensive trials were run, using resistor strain gauges and semiconductor strain gauges, both wired and wireless. With these hand-built systems, various running modes were tested and the results evaluated.

After these trials and an extensive literature search, it was decided to develop a new system based on Surface Acoustic Wave (SAW) devices. As the name suggests, these waves travel very close to the surface of a piezoelectric substrate. Surface Acoustic Wave sensors are extremely versatile devices and have been in use for many years, mainly as filters and delay lines in RF applications [1-3]. They are mass produced at low cost, have a small foot print and high quality factor [4-6]. SAW's utilise Rayleigh waves, named after Lord Rayleigh [7]. In 1885, he was the first person to study and correctly describe analytically the propagation of earthquake waves on the earth's surface. A lesser known application is the use of SAW devices for wireless identification applications [8] and wireless switching [9]. Hybrid Transceivers [10] and even linear motors based on SAW devices have been reported [11, 12]. SAW devices are an important part of most biosensors [13]. However, the most interesting application, for our problem, is the ability to measure strain, temperature and pressure [14-17].

The key to the operation of a SAW device lies in the piezoelectric substrate, which is as follows:

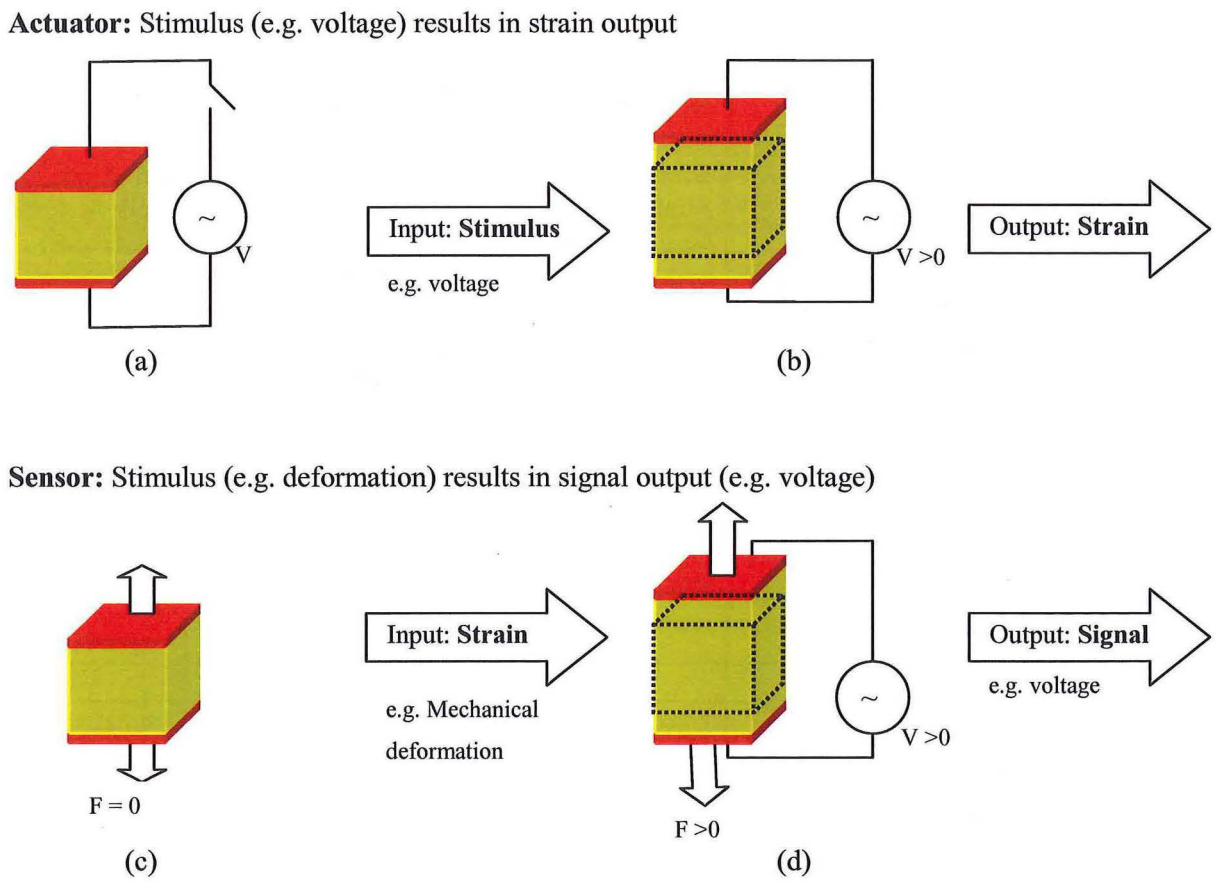

Figure 1: Stimulus-strain relationship for piezoelectric substrate.

Figure 1 illustrates the relationship between stimulus and strain. It is valid for stationary/slowly changing events (i.e. piezoelectric actuator or sensor) and dynamic events (i.e. SAW device excited by an RF

signal). A piezoelectric element working as actuator in its unexcited state is shown in (a). Applying a voltage will lead to a deformation as shown in (b). The same piezoelectric element working as a sensor in its unexcited state is shown in (c). Applying a strain will lead to a deformation and a voltage to be generated as shown in (d).

SAW devices work with their own designed resonance frequency, utilising the piezoelectric effect. Any SAW device is influenced through changing mechanical strain and temperature fluctuations. Because of this, SAW filter and oscillators are isolated from the environment so strain or vibrations will not cause an adverse effect. They are either temperature compensated or kept at constant temperature. On the other hand, changing strain can be used to alter the characteristic of the piezoelectric material. A changing strain will affect the mechanical wave and the signal retransmitted will reflect these changes. For example, if a piezoelectric material is placed on a mechanical part which is used as a stress receptor, the length of the SAW structure will be influenced by changing strain and therefore the delay time will change.

A basic SAW device could look as follows:

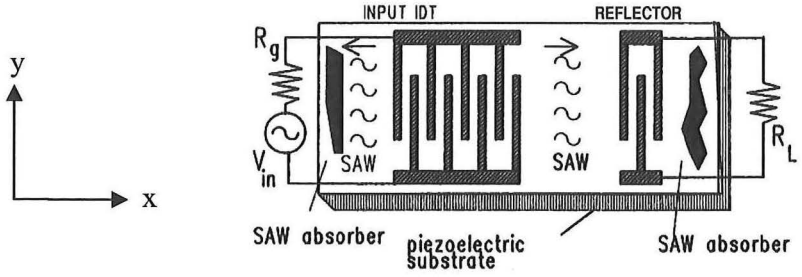

Figure 2: Schematic of basic SAW device with IDT, reflector and absorbers.

Figure 2 shows a basic SAW device, the Input IDT (=Inter Digital Transducer) is generating a mechanical wave which travels in +/- x direction. The IDT on the right hand side could be used as follows:

- Variable resistance connected to reflector (as shown)
- Variable capacitance connected to reflector
- Variable inductivity connected to reflector

Any of these components will have an effect on the reflected signal.

As mentioned earlier, the reflected signal is also influenced by temperature and mechanical strain.

IDTs were invented in 1965 [18] as very efficient devices to generate and detect SAW waves on piezoelectric substrates.

The mechanical wave can be imagined as follows:

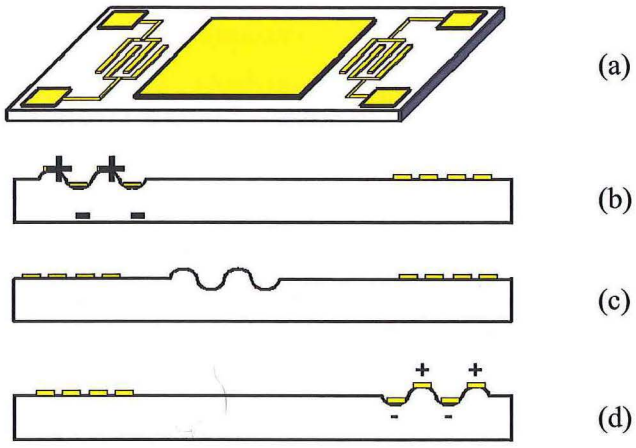

Figure 3: Basic SAW device illustrating distribution of surface acoustic wave.

In Figure 3 the schematic propagation of the surface acoustic wave along the substrate is illustrated. The general arrangement of a SAW device is illustrated in (a) consisting of an Input IDT on the left-hand side, the delay line in the center and the Output IDT on the right-hand side. A short AC voltage pulse applied at the left-hand IDT will generate a mechanical strain and displacement (as of Figure 1) and (b). This displacement forms a wave which travels in +/- x direction as shown in (c) (only + x direction shown). After a short time interval the wave will arrive at the destination (IDT on right hand side) as shown in (d) but will have lost some of its energy. The IDT on the right hand side will convert the wave back into a voltage pulse.

The phase velocity of the mechanical wave and the piezoelectric coupling effect are dependent on the piezoelectric substrate used. A SAW device designed on substrate X will behave differently if fabricated on substrate Y and considerable re-engineering would be necessary to match the performance. Piezoelectric substrates with a high phase velocity will allow higher frequency operation with the same mechanical pitch than substrates with low phase velocity. More information about designing SAW devices in the 10 GHz range is available in [19-21].

The following definitions apply throughout this thesis:

- SAW device: The whole structure as of Figure 2, containing a piezoelectric substrate and the SAW structure. This device could be an oscillator, filter, ID tag (transponder), or sensor.
- SAW structure: Contains generally one or several IDT(s), reflectors, absorbers, antenna, and connectors (see section 1.3).
- IDT: Inter Digital Transducer, which converts a voltage into a displacement of the substrate and ultimately into a surface acoustic wave and vice versa (see Figure 1).

1.1 SAW design guidelines

1.1.1 Rayleigh waves

By definition Rayleigh waves are surface waves. The amplitude decreases exponentially with depth below the material surface. These waves have a two-dimensional cylindrical geometry spread pattern that decreases with radius r from the source proportional to $1/\sqrt{r}$.

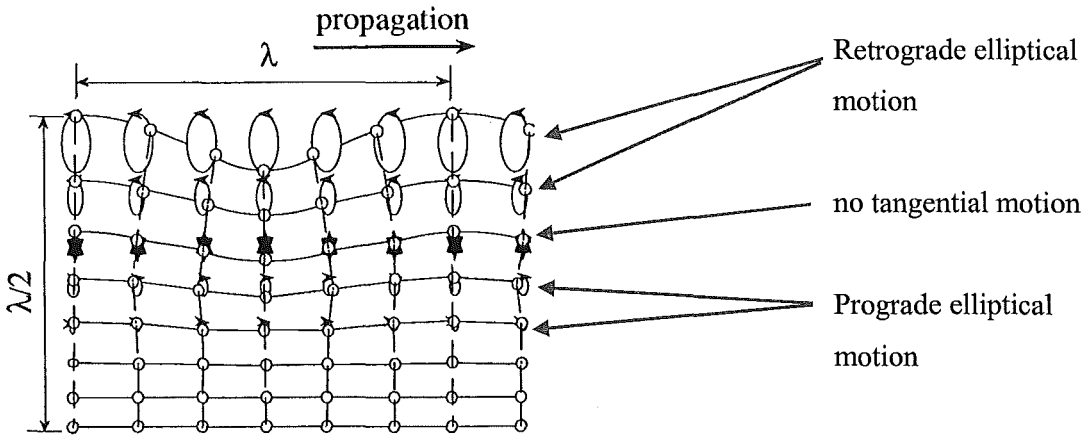

Figure 4: Particle motion of a Rayleigh wave (from [22]).

Figure 4 illustrates the particle motion of the Rayleigh wave. It shows that the wave travels only close to the surface. Rayleigh waves travel along the surface with a retrograde elliptical particle motion (counter clockwise, opposite to wave propagation) and changing to prograde (clockwise, in the direction of the wave propagation) with depth passing through a node where there is no tangential motion at all. Rayleigh wave particle motion is only found in the vertical plane with no tangential motion. An animated graphic showing the particle motion can be found in [23].

1.1.2 Common piezoelectric materials

The most commonly used piezoelectric materials are listed below:

Table 2: Properties of commonly used SAW substrate piezoelectric material cuts.

Material	Orientation		vph	k2	TCD
	Cut	Prop.			
Quartz	ST	X	3158 m/s	0.1%	0
	37° rotY	90° rotX	5094 m/s	0.1%	0
$LiNbO_3$	Y	Z	3488 m/s	4.1%	94 ppm/°C
	41° rotY	X	4750 m/s	15.8%	69 ppm/°C
	128° rotY	X	3980 m/s	5.5%	75 ppm/°C
$LiTaO_3$	36° rotY	Z	4220 m/s	6.6%	30 ppm/°C

where:

Orientation Cut:	Indicates the crystalline orientation of the substrate surface to normal
Orientation Prop:	Indicates the crystalline orientation of the wave propagation direction
vph:	phase velocity
k2:	electro-mechanical coupling coefficient
TCD:	Temperature Coefficient of Delay

1.1.3 General design rules

With regard to SAW design there are no hard and fast rules. In the literature only approximate figures are given and not too many explanations. With the arrival of more powerful computers simulations have been run employing the finite element method (FEM), the boundary element method (BEM) and the spectral domain analysis (SDA) to find optimum design parameters [24, 25]. However, it was decided not to run our own simulations at this stage. Most design rules were obtained from [6] and [26].

The most important design parameters are collated below.

General arrangement of SAW IDT

IDTs are generally built around 50/50 pitch, i.e. the metallic fingers take up 50 % of the area and the gaps in between the other 50%. For some designs the pitch rate is critical as it has an influence on the resonance frequency, but for synchronous resonators this is not an issue. Synchronous resonators, however, have a higher insertion loss than other designs.

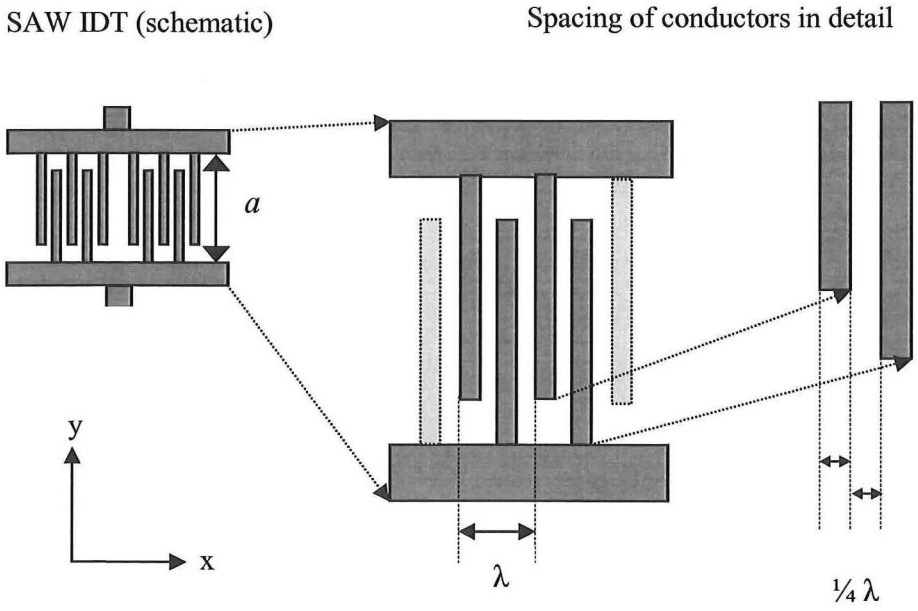

Figure 5: Illustration of SAW device design.

Figure 5 shows the schematic design of a simple SAW IDT, where λ is the acoustic wavelength of the mechanical (SAW) wave and a is the aperture of the IDT.

If we imagine the amplitude of the mechanical wave as a sine wave (in x the direction) then two of the adjacent metal strips (connected to reverse polarity) act as condenser plates in any given time driven by an AC signal. For more details refer to Figure 3.

Acoustic wavelength λ

λ is determined by the phase velocity and the operating frequency as follows: $\lambda = \frac{v_s}{f_{RES}}$

where v_s is the phase velocity of sound and f_{RES} is the center frequency.

Aperture *a*

The aperture a has a similar function as in optical lenses. Generally, the wider a in relation to λ, the more focused the mechanical wave will travel.
a is normally chosen at around 50 λ.

Number of interdigital fingers *n*

The number of interdigital fingers will influence the quality factor of the resulting oscillator. The relative bandwidth $\frac{\Delta f}{f}$ is inverse to the number of periods in the IDTs. A common rule is to keep n at around 50 as a starting point. The influence of n is discussed using simulations in [27].

Metallisation thickness *h*

For the metallisation thickness h only a minimum is given: $h \geq 1\% * \lambda$
This is the minimal required thickness for the IDTs to generate a surface acoustic wave. Another consideration is the required thickness for successful wire bonding (refer to Section 2.8).

1.2 Piezoelectric materials used

1.2.1 Lithium Niobate ($LiNbO_3$)

Lithium Niobate is a ferroelectric material suitable for a variety of applications. Its versatility is made possible by the excellent electro-optic, nonlinear, and piezoelectric properties of the intrinsic material [4, 28]. It is one of the most thoroughly characterized electro-optic materials, and crystal growing techniques consistently produce large crystals of high perfection. Information about technical data and the crystal lattice of $LiNbO_3$ can be found in Chapter 4.

1.2.2 Zinc Oxide (ZnO)

ZnO is a wide bandgap (3.37 eV at room temperature) oxide semiconductor, attracting attention as a potential semiconductor and is a material of choice for MEMS. It exhibits a variety of properties such as semiconductive, photoconductive, piezoelectric, acoustic-optical and electro-optical behaviour [29]. In general, the electrical properties of bulk ZnO are excellent for microelectronic device applications [30, 31]. ZnO has even been synthesised in one-dimensional nanowires in different ways [32-35] and has been successfully deposited as self-organising quantum dots [36] which will initiate new research activities.

1.3 Considerations about conductive material for IDTs and auxiliary conductors

Every SAW device needs a SAW structure: A grid of connectors, called an IDT (which is actually a capacitor) and an auxiliary structure forms the wire bonding pads and an antenna. A general rule is that the metal should be of low resistance and low weight density. Heavy structures will dampen the surface acoustic wave through "mass loading" more than lightweight ones.

Table 3: Commonly used metals for SAW structures.

	Specific resistance at 20°C $\mu\Omega/cm^3$	Specific gravity grams/cm^3
Gold (Au)	2.44	19.32
Nichrome (NiCr)	109.0	8.4
Aluminium (Al)	2.828	2.56 – 2.64
Silver (Ag)	1.629	10.5

Other factors, such as ease of evaporation and adhesion properties also have to be taken into account. Gold is easy to evaporate but needs a NiCr layer to improve adhesion. While Au is one of the best conductors, it is also of high specific gravity. This is a disadvantage, especially for high working frequencies, as it will lead to dampening through mass loading of the acoustic wave and heavy losses. Aluminium, however, is also a very good conductor, but has much lower specific gravity. It is the preferred material for our high-frequency devices. The thicker the connectors, the lower the resistance, but the increasing mass will further dampen the acoustic wave.

1.4 Thesis outline

The remainder of this thesis is structured as follows:

In Chapter 2 details about the experimental techniques employed are presented. Charging problems encountered with Lithium Niobate and solutions are discussed. The fabrication of piezoelectric coatings by sputtering Zinc Oxide is outlined in the latter part of the chapter.

Chapter 3 presents details about the characterisation methods employed.

Chapter 4 describes the fabrication and characterisation of SAW devices on $LiNbO_3$ substrate.

Chapter 5 is devoted to the fabrication and characterisation of SAW devices on sputtered ZnO coatings.

Chapter 6 reviews the previous chapters and suggests aspects for future work.

Chapter 2
Experimental techniques

The most common way to fabricate structures down to the range of nanometres it the so called top-down approach. By using lithographic processes the small nanostructured elements are "machined" from larger pieces. The best known example is microelectronics.

This chapter describes the commonly used techniques employed in this research to fabricate and analyse the SAW devices.

For a comprehensive introduction in all relevant manufacturing techniques, refer to [37].

2.1 Cleaning

Wafers and optical masks need to be perfectly clean. Dust particles as small as 1 μm will have an adverse effect.

The following methods and substances have been used to clean samples and masks from organic and inorganic impurities and depositions.

- Soap in water, scrubbing with Q-tips removes depositions
- Soaking in aqua regia removes inorganic depositions. Aqua regia is a mixture of 1 volume concentrated nitric acid (HNO_3) with 3 volumes of concentrated hydrochloric acid (HCl).
- Plasma cleaning in O_2 in an oxygen asher unit removes stubborn organic depositions
- Solvents (acetone, methylated spirits, isopropyl alcohol) in an ultrasonic bath remove organic depositions and water/moisture

2.2 Computer aided design software

L-Edit® is a Computer aided design (CAD) package and has been used to design the masks for optical lithography as well as patterns for EBL exposures. The Raith 150 electron beam lithography system uses its own editor but allows the import of L-Edit files.

L-Edit is a complete integrated circuit (IC) layout editor with many built-in tools including a design rule checker and a layout extractor [38]. L-Edit can be used for traditional IC design and also for designing microelectromechanical structures (MEMS).

2.3 Optical lithography

Optical lithography uses generally visible light for reproductions, but recently ultraviolet (UV) and deep ultraviolet (DUV) have been introduced to reproduce smaller features.

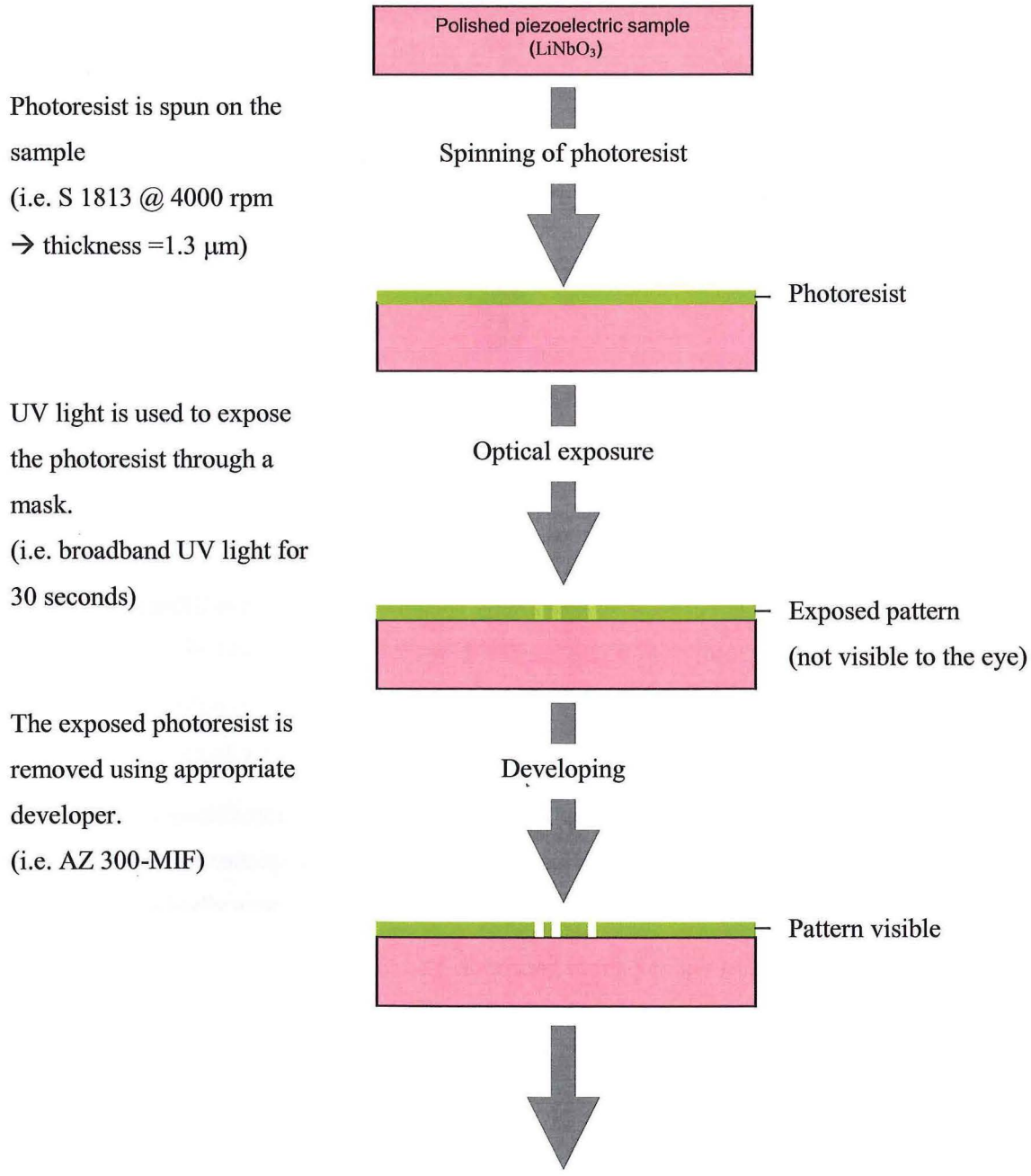

Figure 6: Optical lithography fabrication sequence (part I).

Aluminium or gold (used as electrodes) is evaporated on the surface.

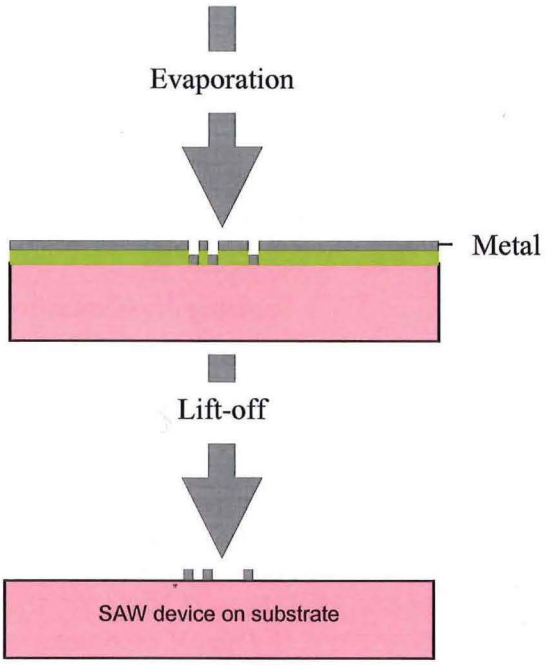

The photoresist is removed using acetone. The metal will only remain on those places where the photoresist was exposed and removed.

Figure 7: Optical lithography fabrication sequence (part II).

The optical lithography fabrication sequence as commonly used the this research is illustrated in Figure 6 and Figure 7.

Mask making

The first step in optical lithography is to create a mask, which is commonly borosilicate glass or fused silica. A resist coating is applied to the mask substrate. This is done using a spinner which spreads the resist into a uniform coating. To mechanically "fix" the resist, it undergoes a prescribed baking operation.

The next step is to pattern the resist with a pattern generator. The source for traditional optical lithography is a mercury arc lamp. After patterning, the mask is developed and a metal coating (commonly chromium) is applied. The chromium fills the voids in the developed resist, as well as on top of the undeveloped resist. The resist is then stripped away, leaving a pattern of chromium on the mask substrate. Prior to use, the mask must be inspected and if necessary repaired.

Masks for optical lithography were designed using L-Edit and fabricated at Industrial Research Limited, Lower Hutt.

Lithographical reproduction

A similar process is performed on the substrate and resist to be patterned for the final structures. The mask is used analogous to a photographic negative and the mask pattern is transferred into the resist carried on the substrate. Normally, the mask is held in very close proximity to the substrate and resist (proximity or shadow printing).

After exposure, the substrate resist is developed similar to the mask resist leaving openings in the resist. This allows access to the substrate for further etching, deposition, or doping.

2.4 Electron Beam lithography (EBL)

Introduction

Electron beam lithography (EBL) is a technique for creating extremely fine patterns (sub micrometer features, down to 10 nm) for integrated circuits and masks. This is possible due to the very small spot size of the electrons, as opposed to optical lithography where the resolution is limited by the wavelength of light used for exposure. The electron beam has a wavelength so small that diffraction no longer defines the lithographic resolution.

The most important use of EBL is in photo mask production. Masks are made by coating a chrome clad glass plate with electron-beam sensitive resist layer which is subsequently exposed, developed, and etched to generate the required pattern on the mask.

The second application is the direct write for advanced prototyping of integrated circuits and manufacture of small volume specialty products, such as gallium arsenide integrated circuits and optical wave-guides.

Another field is research into the scaling limits of IC's and studies of quantum effect devices and other novel physics phenomena at very small dimensions.

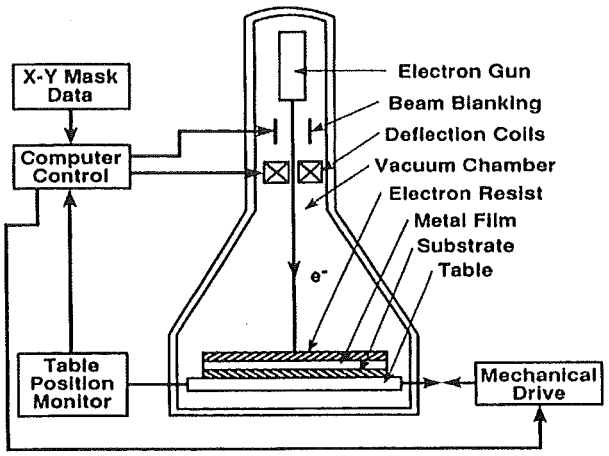

Figure 8: Overview of electron-beam exposure system.

Figure 8 shows a typical configuration of an EBL system containing a vacuum chamber with the electron gun and deflection coils and a mechanical drive to position the sample as well as a computer controlled pattern generator.

Electron Beam Lithography utilises the fact that certain chemicals change their properties when irradiated with electrons just as a photographic film does when irradiated with light. The electron beam is generated in a Scanning Electron Microscope which normally is set up to provide an image of an object by rastering with a focused beam of electrons over it. Collecting the electrons that are scattered or emitted from that object at each raster point provides an image. With computer control of the position of the electron beam it is possible to write arbitrary structures onto a surface. With our Raith 150 electron beam lithography system achievable resolutions go to the order of 20 nm.

Photo resist

For this research, Poly Methyl Methacrylate (PMMA) photo resist was used. PMMA is a high resolution positive photo resist for direct write E-beam as well as x-ray and deep UV lithography processes [39]. PMMA has been used as a bilayer system, the first coat is of low molecular weight, LMW PMMA (4%), and the second coat is of high molecular weight, HMW PMMA (2.5%). This ensures an undercut during development for better lift-off, as LMW PMMA is attacked more vigorously by the developer.

LMW PMMA (4%) and HMW PMMA (2.5%) were both spun with 4000 rpm which results in a thickness of around 160 nm and 40 nm, respectively.

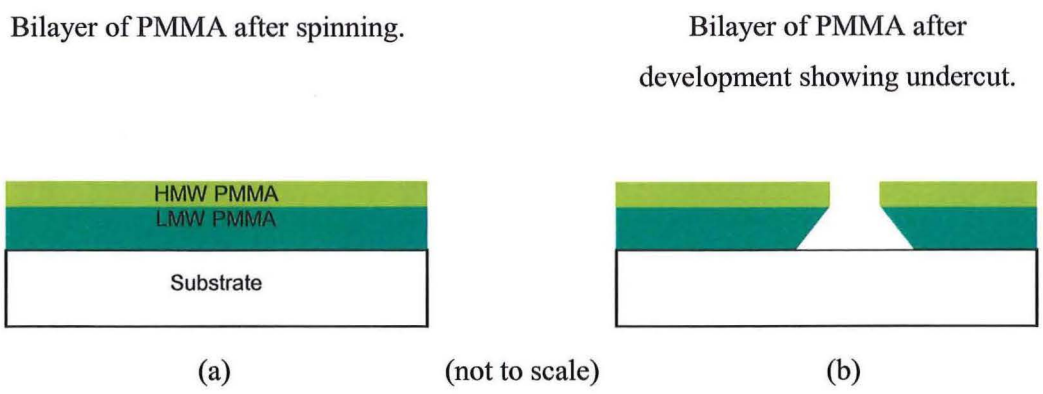

Figure 9: Overview of bilayer PMMA resist showing undercut after development.

Figure 9 shows the structure of bilayer PMMA after spinning in (a) and the undercut which occurs during development in (b). This undercut in the structure aids the lift-off at the end of the fabrication. For more information about fabrication using PMMA refer to the figure below.

Fabrication sequence using EBL

This sequence is an introduction in fabricating small scale patterns using EB lithography on rods or another suitable substrate.

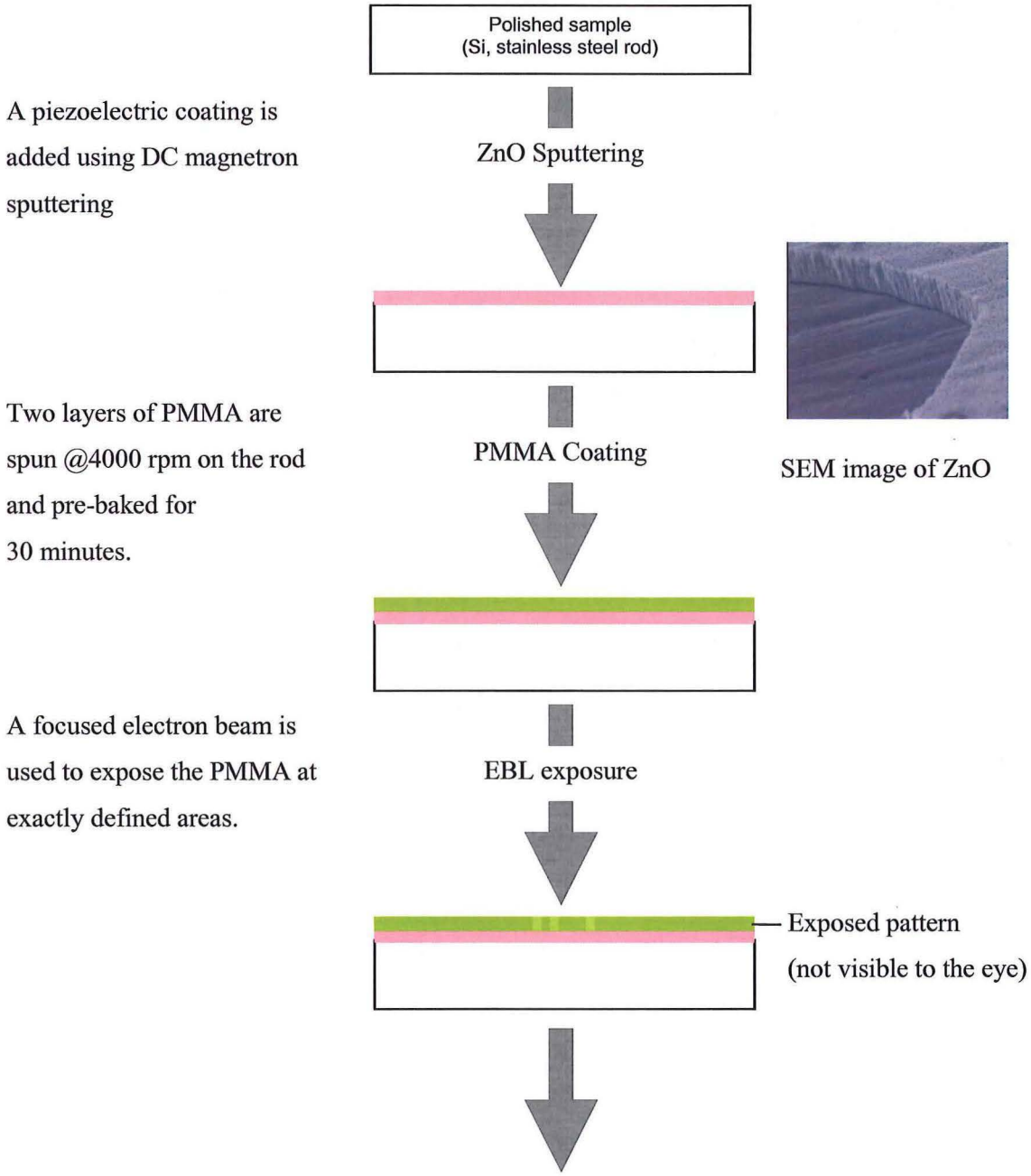

Figure 10: EBL fabrication sequence (part I).

The exposed PMMA is removed using appropriate developer.

Developing

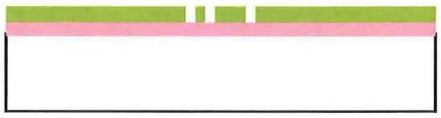

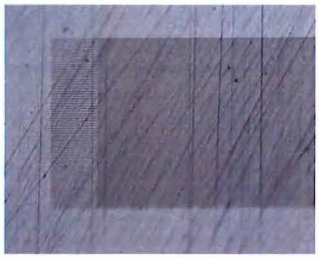

Optical microscopy image of IDT

Aluminium (used as electrodes) is evaporated on the surface.

Al Evaporation

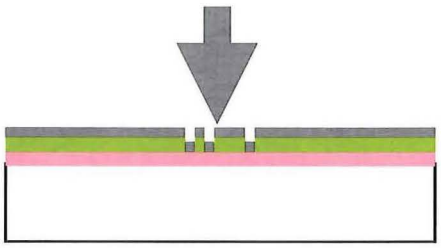

The PMMA is removed using acetone. The aluminium will only remain on those places where the PMMA was exposed.

Lift-off

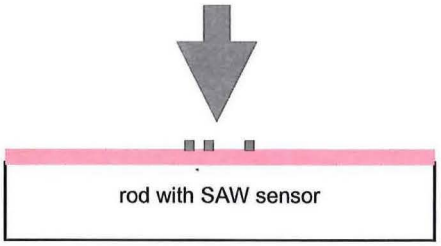

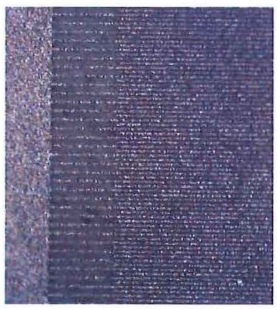

Optical microscopy image of IDT

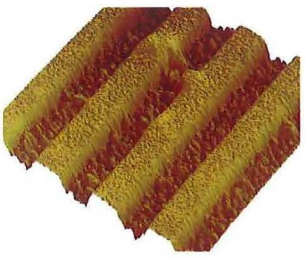

AFM image of IDT

Figure 11: EBL fabrication sequence (part II).

2.5 Vacuum thermal evaporation

In this technique, a metal is evaporated under vacuum. A current flows through a filament or boat containing the metal to be deposited and heats it to a very high temperature, until it evaporates (depending on vapour pressure and melting point). The material vapour finally condenses in form of a thin film on the cold substrate surface and on the vacuum chamber walls. The pressure is kept at around 10^{-4} Pa, to avoid reaction between the vapour and residual gas atmosphere. At this low pressure, the mean free path of the vapour atoms is the same order as the vacuum chamber dimensions, so these particles travel in straight lines from the evaporation source towards the substrate. This leads to 'shadowing' phenomena with 3D objects, especially in those regions not directly accessible from the evaporation source. Steep sidewalls of developed structures will not be coated. The average energy of vapour atoms reaching the substrate surface is generally low (order of kT, i.e. tenths of eV). This seriously affects the morphology of the films, often resulting in a porous and weakly adherent material.

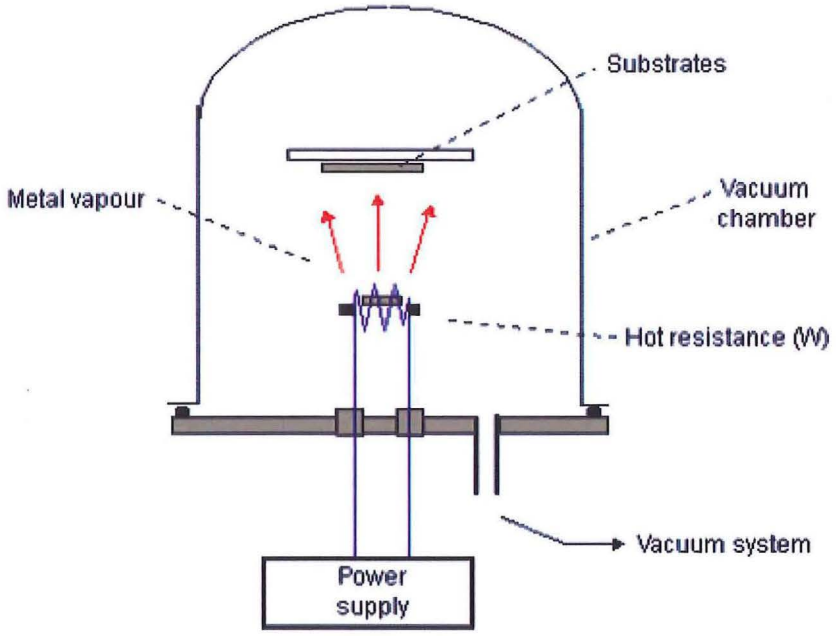

Figure 12: Schematic diagram of a vacuum thermal evaporation system.

In thermal evaporation techniques, different methods can be applied to heat the material. The equipment in the laboratory use either resistance heating (Joule effect) or bombardment with a high energy electron beam, usually several KeV, from an electron beam gun (electron beam heating)

For this work the Balzers evaporation system with resistive heating has been used.

Figure 13: Balzers thermal evaporation system.

2.6 Lift-off

After defining a pattern using optical lithography or EB lithography and the deposition of a metallic film all over the substrate, lift-off is initiated as follows: The photo resist under the film is removed with solvent, taking the film with it, and leaving only the film which was deposited directly on the substrate. Depending on the type of lift-off process used, patterns can be defined very accurately and for very fine geometries.

2.7 Wet etch

During wet etching, deposited material on a substrate is removed by immersing the wafer in a liquid bath of chemical etchant. Wet etchants fall into two broad categories; isotropic etchants and anisotropic etchants. Isotropic etchants attack the material being etched at the same rate in all directions. Anisotropic etchants attack the substrate at different rates in different directions, and so there is more control of the shapes produced [40]. Potassium hydroxide (KOH) is an anisotropic etchant and has been used for this work.

2.8 Wire bonding

Wire bonding is used for electrical interconnection between the SAW device and external circuit using thin wire and a combination of heat, pressure and/or ultrasonic energy. Wire bonding is a solid phase welding process, where the two metallic materials (wire and pad surface) are brought into intimate contact. Once the surfaces are in intimate contact, electron sharing or interdiffusion of atoms takes place, resulting in the formation of a wire bond. In the wire bonding process, bonding force can lead to material

deformation, breaking up of the contamination layer and smoothing out of the surface asperity, which can be enhanced by the application of ultrasonic energy. Heat can accelerate interatomic diffusion and the bond formation.

The wire bonding machine used for this research requires generally a metal thickness of at least 50 nm.

2.9 Charging problems on $LiNbO_3$

$LiNbO_3$ is not only piezoelectric (a mechanical strain generates a voltage) but also pyroelectric (changing temperature generates a voltage). A charged wafer leads to various problems, such as sparks, which can destroy structures (IDT) or make it hard to work with. While optical lithography was a success, EBL however, was tricky. As an example, it was hard to spin photo resists evenly, which is a requirement for good reproduction. During EBL, the charge (bombardment of electrons) cannot be dissipated. This leads to a built up of charge which in turn will deflect the electron beam.
The following procedures have been evaluated to minimise charging problems and are discussed below:

- Use of conductive polymers
- Coating of thin Au
- "Reducing" of wafer

2.9.1 Using conductive polymers for charge dissipation

The conductive polymer used is a mixture of PEDOT : PSS, dispersed in water. It is designed to increase the conductivity of an insulating surface.

Table 4: Details of the conductive polymer used for charge dissipation.

Synonym / Abbreviation	PEDOT/PSS
Formula	H_2O; $[\text{-}C_6H_4O_2S\text{-}]_x^{0.33+}$ / $[\text{-}CH_2CH(C_6H_4SO_3)\text{-}]^{-0.33x}$
Chemical Name	Poly(3,4-ethylenedioxythiophene)/poly(styrenesulfonate) aqueous dispersion

The wafer was, as usual, coated with LMW (4%) PMMA and HMW (2.5%) PMMA. After baking the resist a conductive polymer was spun and baked. Subsequently the sample was exposed and developed. The result was slightly better, but there was still some drift noticeable.

Fabrication:

- Cleaning of wafer (as of section 2.1)
- Spin LMW PMMA (4000 rpm, 1 minute), pre-bake (185 °C, 30 minutes)
- Spin HMW PMMA (4000 rpm, 1 minute), pre-bake (185 °C, 30 minutes)
- Spin conductive layer (2000 rpm, 30 seconds), pre-bake (95 °C, 10 minutes)
- EBL exposure
- Wash conductive layer away (H_20)
- Develop PMMA (using 1:3 Methyl Isobutyl Ketone (MIBK): IsoPropyl Alcohol (IPA), 30 seconds)

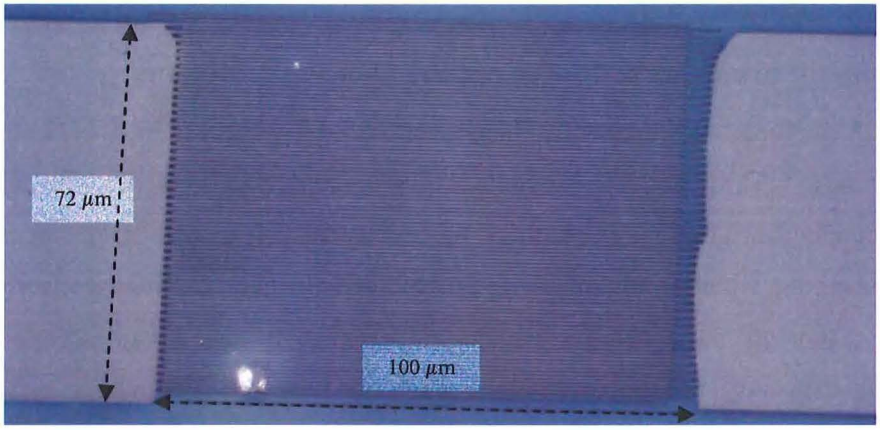

Figure 14: Optical microscope image of SAW IDT showing drift.

Figure 14 shows slight drifting after EBL exposure and lift-off (structure should be right-angled) and some charging marks. This is one of the best IDTs fabricated on the Philips EBL. The line thickness is 360 nm and the period is 720 nm.

Another sample was prepared using the conductive polymer before applying a bilayer of PMMA which did not lead to any improvements.

2.9.2 Using gold for charge dissipation

The wafer was coated with LMW PMMA and HMW PMMA. After baking, a 10 nm Au-layer was evaporated onto the resist.

Subsequently the sample was exposed and developed. No charging was detected.

Fabrication:

- Cleaning of wafer (as of section 2.1)
- Spin LMW PMMA (4000 rpm, 1 minute), pre-bake (185 °C, 30 minutes)
- Spin HMW PMMA (4000 rpm, 1 minute), pre-bake (185 °C, 30 minutes)
- Evaporate Au (10 nm)
- EBL exposure with SAW structure
- Use KOH gold etch (20 sec) to remove Au, rinse in DI water
- Develop PMMA (using 1:3 MIBK:IPA, 30 seconds)

The disadvantage of this treatment is that alignment marks cannot be seen during EBL alignment.

2.9.3 Pre-treatment of $LiNbO_3$ wafers to reduce charging problems

A procedure has been reported, whereby the wafer gets chemically reduced in H_2/N_2 forming gas under elevated temperatures [41]. Chemical reduction of lithium niobate yields crystals with enhanced electrical conductivity and optical absorption. The higher conductivity of such crystals makes them less susceptible to pyroelectric charging, which would otherwise present difficulties in SAW device fabrication and operation. The crystals' increased near-ultraviolet light absorptivity allows improvements in photolithographic exposure, such as generating narrower and more precise lines.

One preliminary trial was carried out in the University of Canterbury Physics Department using their custom made furnace. A quartz glass tube containing a small sample (20 by 20 mm) was inserted into a small furnace. The volume was flushed with N_2 a couple of times to remove any residual oxygen and then filled with H_2/N_2 and kept under a slight vacuum. The ratio was manually set at 10% H_2 to 90% N_2. The tested sample did not show any charging and spinning trials have been promising. EBL trials however showed that charging was still evident.

After the commissioning of a new furnace in our department, two more trials were run. On the first trial, the chamber was preheated to 400 °C and pre-flushed with forming gas (5% H_2/95% N_2). The wafer was added and left for 90 minutes while forming gas was admitted. After that, the wafer was immediately removed. After cooling down, there were still charging effects.

For the second trial the wafer was put in the cold furnace and the forming gas immediately admitted. The temperature was slowly raised to 600 °C and kept at this level for two hours. After that, it was allowed to cool down to room temperature when the forming gas was switched off. The wafer showed a slight discoloration (oxidation layer). No charging was evident. The wafer was quickly heated to 185 °C and cooled to room temperature and showed no sign of charging. EBL trials have been successful.

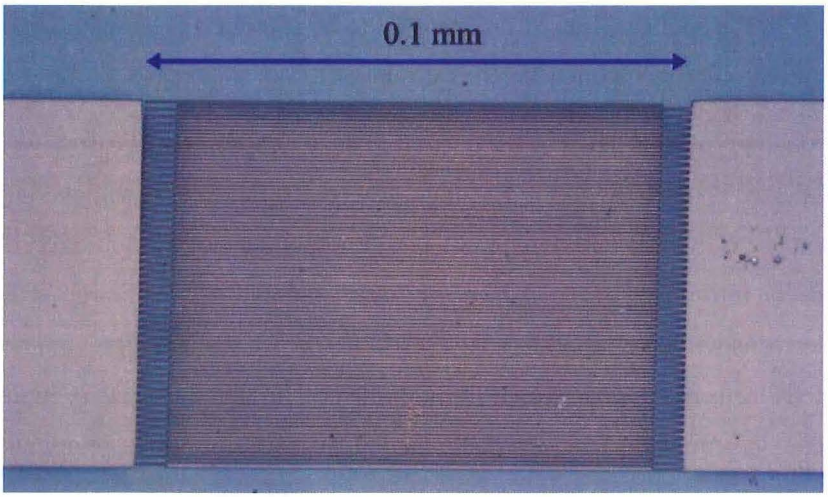

Figure 15: Optical microscope image showing SAW IDT fabricated after reducing of wafer.

Figure 15 shows an IDT fabricated on $LiNbO_3$. The structure is well reproduced and no charging is evident but unfortunately the IDT had a short and could not be tested.

2.10 Thin film sputtering of piezoelectric ZnO

2.10.1 Introduction

Thin film coatings can be deposited by means of sputtering. Sputtered thin films have generally a thickness between a few nanometres and a few micrometers.

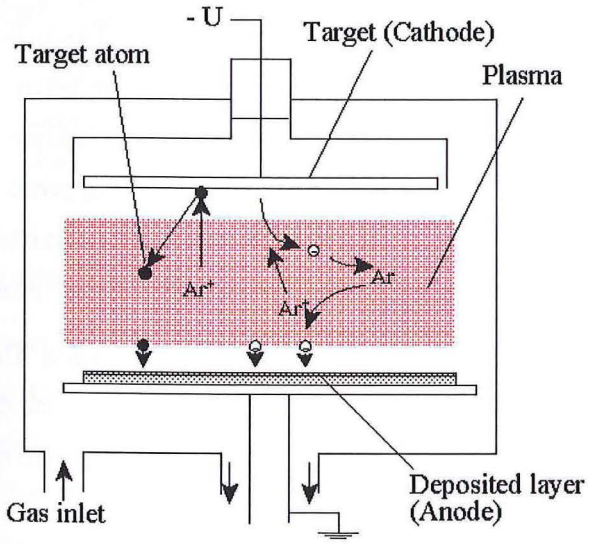

Figure 16: Schematic diagram of the sputtering chamber.

As shown in Figure 16 the sputter target of the material to be sputtered is the cathode of the system and the substrate/substrate holder the anode (which is grounded).

Once the vacuum chamber is evacuated to the desired level, a sputtering gas (usually Argon) is introduced. The pressure is normally in the Pa range. Reactive sputtering is achieved by adding O_2 to form oxides or H_2 to form hydrogenated material. The stoichiometry of the sputtered film can be set by varying the ratio of the introduced gases. A large negative potential between target and ground initiates the process and electrons will be emitted from the target surface. Typical voltage ranges from 100 Volts to 1 kV. The ejected electrons are accelerated through the potential and get a very high kinetic energy. They collide with the gas molecules and ionise them. The positive ions are accelerated towards the cathode. On hitting the target surface, part of the energy is transformed into heat and part is transferred to other particles. These particles can eventually get enough energy to leave the target surface. Various particles are eventually emitted: neutral atoms which will eventually reach the substrate and build the film, negative ions, photons and secondary electrons. The secondary electrons will again be accelerated from the target and ionise more gas atoms that will sputter the target and so on. The secondary electron yield needs to be high enough in order to maintain the plasma.

When the substrate is immersed into the plasma (shutter removed), the electrons cover the surface much faster than the ions. A negative potential develops, which attracts the ions and repels the electrons. Around the substrate, an electron depleted sheet forms up to a steady state when the ionic current equals to the electron current. The target has always the strongest negative potential.

The bombardment is a key parameter in the sputtering deposition. It has at least three major effects. Firstly, it heats the substrate. The temperature of a substrate immersed in plasma will rise up to 150 °C. This thermal energy enhances the surface mobility of the atoms and has an influence on the growth of the film. Secondly, the energy of a bombarding particle can be directly transferred to an atom of the surface through momentum transfer in a collision. It will also increase its mobility which can lead to resputtering of the atom from the surface. Thirdly, if the energy of the bombarding particle is too high, it can damage the film by the creation of defects during its implantation in the film. The bombardment is also influenced by nature and pressure of the sputtering gas, the sputtering distance, and the sputtering angle.

Today, most commercial sputtering systems use planar magnetron targets. This technology uses powerful magnets to confine the "glow discharge" plasma to the region closest to the target plate. That vastly improves the deposition rate by maintaining a higher density of ions, which makes the electron/gas molecule collision process much more efficient.

2.10.2 ZnO sputtering

In this work, *reactive magnetron* sputtering has been used. *Reactive* sputtering means that an oxide film is grown by the sputtering of a metallic target (Zn) in an oxidising atmosphere. *Magnetron* sputtering utilises magnetic cathodes which trap the secondary electrons in the magnetic field close to the target. This technique increases the sputtering yield of the cathode and allows the use of lower pressures during the process for improved film finish.

For our intended use, ZnO should have the following properties:

- Preferred crystal structure ([002] orientation, crystal growth normal to surface)
- Highly insulating properties
- Smooth and uniform deposition
- Piezoelectric characteristic

ZnO can be sputtered on a wide range of materials and on irregularly shaped objects. Sputtered ZnO films show, with a proper fine-tuning of parameters, a natural tendency to grow with a preferred [002] orientation, which is necessary for the coating to be piezoelectric.

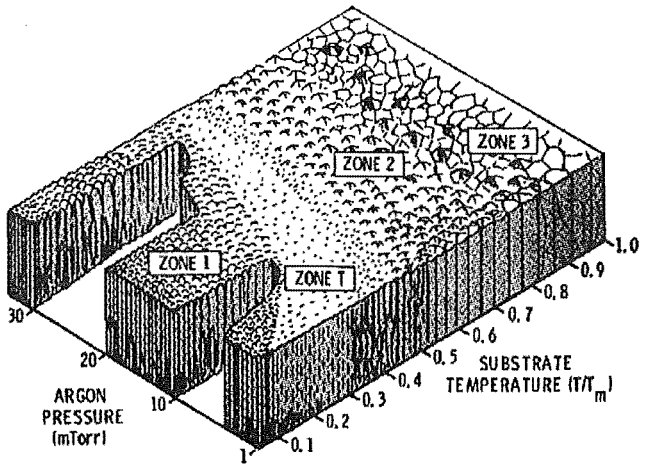

Figure 17: Microstructure zone diagram for metal films deposited by magnetron sputtering [42].

Figure 17 shows the microstructure zone diagram of metal films deposited by magnetron sputtering. T is the substrate temperature and T_m is the coating material melting point. It clearly illustrates that Zone 1 is the desired working area during sputtering. That is columnar growth of individual crystals defined by voided growth boundaries. These voided growth defects are a consequence of atomic shadowing. Shadowing induces open boundaries because high points on the growing surface receive more coating flux than valleys, particularly when a significant oblique component is present in the flux [42]. This means, a low sputtering temperature and the proper pressure range are critical to achieve the proper crystal composition.

It has to be noted that ZnO would contaminate semiconductor fabrication equipment through its oxygen content. A simple way around this is the application of a passivation layer. A thin silicon nitride layer covers the ZnO layer and prevents contamination [43].

2.10.3 Description of sputtering system

The BOC Edwards Auto 500 is a versatile, front-loading thin film system for research & development or pre-production. The box chamber allows it to perform a combination of evaporation, electron beam, and sputtering applications on large-diameter substrates, without breaking the vacuum.

The system contains:

① Electron beam evaporation source with four selectable crucibles and shutter
② DC sputtering target and shutter
③ RF sputtering target and shutter
④ Mass flow control panel for two gasses
⑤ Substrate heater
⑥ Rotary work holder
⑦ Crystal thickness monitor

(a) (b)

Figure 18: Overview of BOC Edwards Auto 500 Sputtering system

In Figure 18 an overview of the sputtering system is shown in (a) and a view of the components in the vacuum chamber in (b).

Chapter 3
Characterisation methods

3.1 Evaluation of the piezoelectric quality of sputtered ZnO

Sputtering ZnO is a more or less straight forward task. However, proving that the sputtered coatings meet the requirements for piezoelectricity requires considerable effort.

The following tests have been done on various samples and are described later in this chapter:

- Rutherford backscattering (RBS)
  Counting of collisions between ions and atoms
- X-ray diffraction (Debye Scherrer method)
  Identification and quantitative determination of various crystalline compounds in a sample
- Resistance measurement
  Determination of electrical resistance of a sample using current-voltage relationship
- Scanning Electron Microscopy (SEM) imaging
  Surface analytical technique, imaging of surfaces using a scanned electron beam
- Atomic force microscope (AFM) imaging
  High resolution surface scanning of sample using small tips

The most important characteristic of the piezoelectric films sputtered is the piezoelectric coefficient d_{33}. The displacement induced by an electric field is in the 0.01 nm to 0.1 nm range.

The following methods are usually employed:

- $e_{31,f}$ determination for PZT films using a conventional 'd_{33}' meter [44]
- Double beam interferometer [45], [46]
- Plank method [47]

Unfortunately, none of these tests to measure the piezoelectric properties d_{33} could be carried out in our laboratory as the necessary apparatus were not available.

3.1.1 Rutherford Backscattering

Rutherford backscattering (RBS) is based on collisions between atoms and derives its name from Lord Ernest Rutherford, a New Zealander. In 1911 he was the first to present the concept of atoms having nuclei.

Light ions (He^+) are beamed to the material surface of a sample. By measuring the number and energy of ions in the beam which backscatter after colliding with atoms in the near-surface region of the sample, it

is possible to determine atomic mass and elemental concentrations versus depth below the surface. RBS is ideally suited for determining the concentration of trace elements heavier than the major constituents of the substrate. Its sensitivity for light masses, and for the makeup of samples well below the surface, is poor.

When a sample is bombarded with a beam of high energy particles, the vast majority of particles are implanted into the material and do not escape. This is because the diameter of an atomic nucleus is of the order of 10^{-15} m while the spacing between nuclei is of the order of 2×10^{-10} m. A small fraction of the incident particles do undergo a direct collision with a nucleus of one of the atoms in the upper few micrometers of the sample. This "collision" does not actually involve direct contact between the projectile ion and target atom. Energy exchange occurs because of Coulomb forces between nuclei in close proximity to each other. However, the interaction can be modelled accurately as an elastic collision using classical physics.

The energy measured for a particle backscattering at a given angle depends upon two processes. Particles lose energy while they pass through the sample, both before and after a collision. The amount of energy lost is dependent on that material's stopping power. A particle will also lose energy as a result of the collision itself. The collision losses depend on the masses of the projectile and the target atoms. The ratio of the energy of the projectile before and after collision is called the kinematical factor.

The number of backscattering events that occur from a given element in a sample depend upon two factors: the concentration of the element and the effective size of its nucleus. The probability that a material will cause a collision is called its scattering cross section.

RBS measurement were done at the Institute of Geological and Nuclear Sciences, Lower Hutt.

3.1.2 X-ray diffraction (Debye Scherrer)

X-ray diffraction is a versatile, non-destructive analytical technique for identification and quantitative determination of the various crystalline compounds, known as 'phases', present in solid materials and powders. Identification is achieved by comparing the X-ray diffraction pattern - or 'diffractogram' - obtained from an unknown sample with a database containing reference patterns. In our case, we simply compared the measured values with values of ZnO powder contained in a database. Results using this method can be compared with given materials.

X-ray diffraction measurements were done in the Geochemistry laboratory at the University of Canterbury.

3.1.3 Resistance measurement

The resistance across two probes was measured using the Semiconductor Parameter Analyser HP 4155A and the probe station. This is an approximate measurement only. Generally the shape of the contact electrodes and the manual positioning does not allow repeatable positioning with regard to distance between the electrodes and the contact area. The distance between the two probes was kept at 8 mm.

Figure 19: Semiconductor Parameter Analyser HP 4155A with probe station in background.

3.1.4 SEM imaging

Scanning electron microscopy (SEM) is a widely used surface analytical technique. SEM, accompanied by X-ray analysis, is considered a relatively rapid, inexpensive, and basically non-destructive approach to surface analysis. High resolution images of surface topography, with excellent depth of field are produced using a highly-focused, scanning (primary) electron beam. The primary electrons enter a surface with high energy, and generate many low energy secondary electrons. The intensity of these secondary electrons is largely governed by the surface topography of the sample. An image of the sample surface can thus be constructed by measuring secondary electron intensity as a function of the position of the scanning primary electron beam. High spatial resolution is possible because the primary electron beam can be focused to a very small spot (< 10 nm). High sensitivity to topographic features on the outermost surface (< 5 nm) is achieved when using a primary electron beam with an energy of < 1 keV. In addition to low energy secondary electrons, backscattered electrons and X-rays are also generated by primary electron bombardment.

We used the SEM microscopes both at Mechanical Engineering (JEOL JSM 6100) and at Plant and Microbial Sciences (Leica 440), and more recently the Raith 150 in our department.

Conductive samples sputtered with ZnO were directly placed on a sample holder. Charging problems became more or less apparent, depending on the thickness of the coating.

3.1.5 Atomic force microscope (AFM) imaging

An AFM utilises a sharp probe moving over the surface of a sample in a raster scan. The probe is basically a tip on the end of a cantilever which bends in response to the force between the tip and the sample. As the cantilever flexes, the light from a laser is reflected onto the split photo-diode. By measuring the difference signal (A-B), changes in the bending of the cantilever can be measured. Since the Cantilever obeys Hooke's Law for small displacements, the interaction force between the tip and the sample can be found.

The movement of the tip or sample is performed by an extremely precise positioning device made from piezo-electric ceramics, most often in the form of a tube scanner. The scanner is capable of sub-angstrom resolution in x-, y- and z-directions. However, some limiting factors have to be taken in account. Depending on the tip shape, the resolution will be limited as a tip is not able to profile sides of surfaces steeper than the sidewall angle of the tip. For more information refer to [48].

For this project, the department's AFM, a Digital Instruments 3100 has been used.

3.2 Testing of SAW devices with interrogator

Surface acoustic waves can be detected by the following means:

- Nanoscale investigation of longitudinal surface acoustic waves [30]
- Piezoresistive detection of acoustic waves (indirect method) [49]

However, these methods were not at our disposal.

Interrogation Unit

SAW devices are commonly scanned by an Interrogation unit. A high frequency burst signal emitted from the interrogation unit is received by the antenna of the SAW device. The interdigital transducer (IDT) transforms this signal to a surface acoustic wave in the piezoelectric substrate. This wave skims along the surface of the substrate and the reflectors placed in its path will reflect parts of the incoming wave. After some time, the reflected wave will be converted back to an electrical signal by the IDT and sent back to the request unit. The response signal contains a unique identification (depending on the number of reflectors and their distances from the IDT).

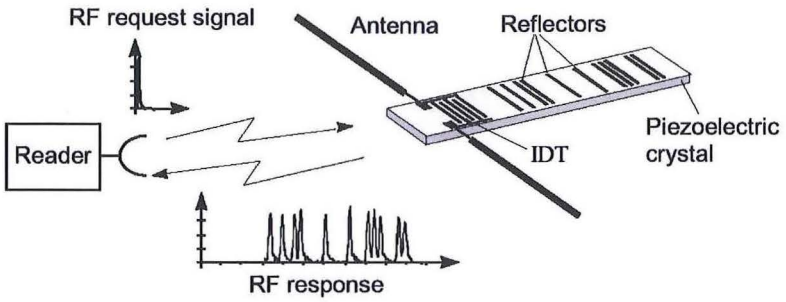

Figure 20: Interrogated SAW device.

Figure 20 illustrates a schematic drawing of a passive SAW ID tag which is interrogated by a radio request unit.

It has to be noted that the radio waves travel with the speed of light (3×10^8 m/s) between the reader and the antenna of the SAW device, while the surface acoustic waves on the SAW device travel with the characteristic phase velocity (typically 3×10^3 m/s). A changing distance between reader and interrogated SAW device does not alter the measured delay times to a great deal, as the radio waves travel in the order of 100000 times faster than the surface acoustic wave.

The request unit consists of a Network analyser HP 8753D and a tuned $\frac{\lambda}{4}$ antenna on a ground plane.

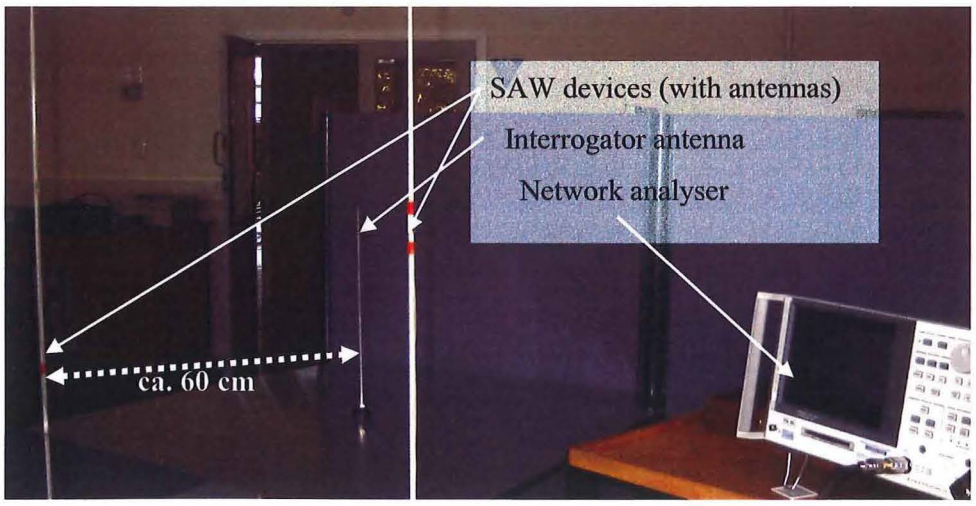

Figure 21: Interrogation setup showing network analyser, antenna and two SAW devices.

Figure 21 shows the arrangement used to interrogate the SAW devices. The signal generated by the network analyser is radiated off the antenna on the center of the ground plane. The SAW devices with antenna are mounted on fibreglass rods. The distance between interrogator antenna and the SAW devices is around 60 cm. All these measurements were performed in a "normal" lab with no specific shielding (such as faraday cage) in place.

This particular model is a vector analyser and allows the direct conversion of measurement into the time domain.

Setup of network analyser

In order to interrogate a SAW device the center frequency of the network analyser is set to the expected resonance frequency and the bandwidth to around 20%. A high bandwidth is needed for accurate Inverse Fourier transformation (Conversion of reflected signal, which is in the frequency band into the time domain). The mode is set to S_{11} measurement which records the reflection losses of the device under test. The output power is set at 10 dBm at the output of the network analyser.

The inbuilt RF generator generates a chirp signal with discrete frequencies emitted from the low end to the high end of the band (usually in 201 discrete steps).

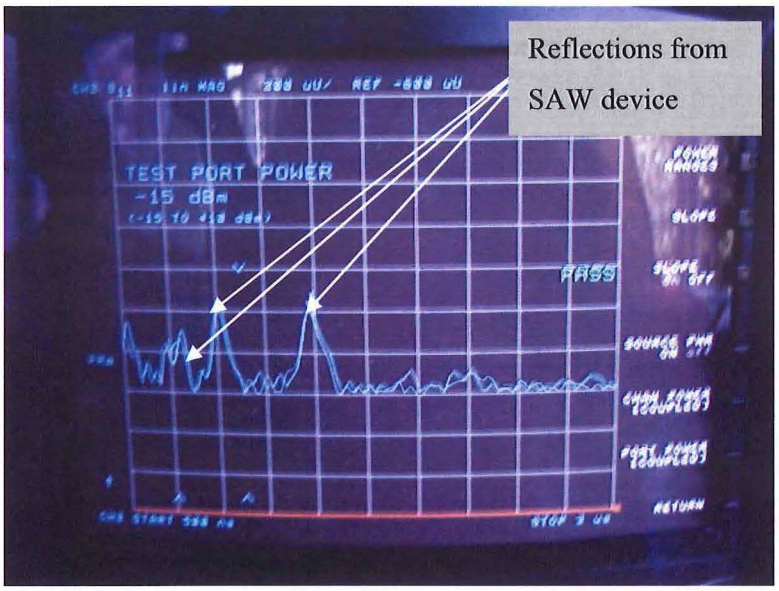

Figure 22: Reflections measured off SAW device.

A picture taken from the network analyser is shown in Figure 22. The x-axis shows the time delay of the reflected signal in a range from zero to 3 μs and the y-axis represents the amplitude of the signal (in logarithmic scale). It shows the inverse Fourier transformed spectrum that was measured on the antenna (reflected from SAW ID tag). Several peaks appear at around 0.8 μs, 1 μs, and 1.5 μs. A large reflected signal (reflection of antenna) which occurs after a short delay (< 200 ns), is not shown.

During this research the focus was to get working SAW devices, the wireless range achieved was secondary. Therefore the measurements were not compared quantitative but qualitative.

Another student is currently working on a separate research project which aims to develop a low cost interrogator for the fabricated SAW devices both in the 180 MHz and 2.45 GHz range.

Chapter 4

Fabrication and characterisation of SAW devices on $LiNbO_3$ substrate

These first SAW devices were created to gain further knowledge about the various manufacturing steps and achievable wireless range for interrogation. Technical limits, such as in optical lithography were avoided so modest values for frequency and structure size were chosen.

These devices were fabricated on single crystal Lithium Niobate ($LiNbO_3$) which is a strong piezoelectric material.

Table 5: Technical details of single crystal $LiNbO_3$.

Supplier	Crystal Technology, Inc.
Part Number	99-30003-01
Size (diameter)	2.995" +0.010", -0.015"
Thickness	0.0197" ±0.0010"
Axes Orientation	127.86° surface normal oriented perpendicular to the major face ±15' X-axis x-ray oriented perpendicular to a 0.900" ±0.080" reference flat within ±15'. A 0.400" ±0.110" secondary flat at 90° to the reference flat.
Crystal structure	Trigonal, space group R3c
Cell parameters	a=5.148Å, c=13.863Å

See [4] for full technical specifications.

Crystal lattice

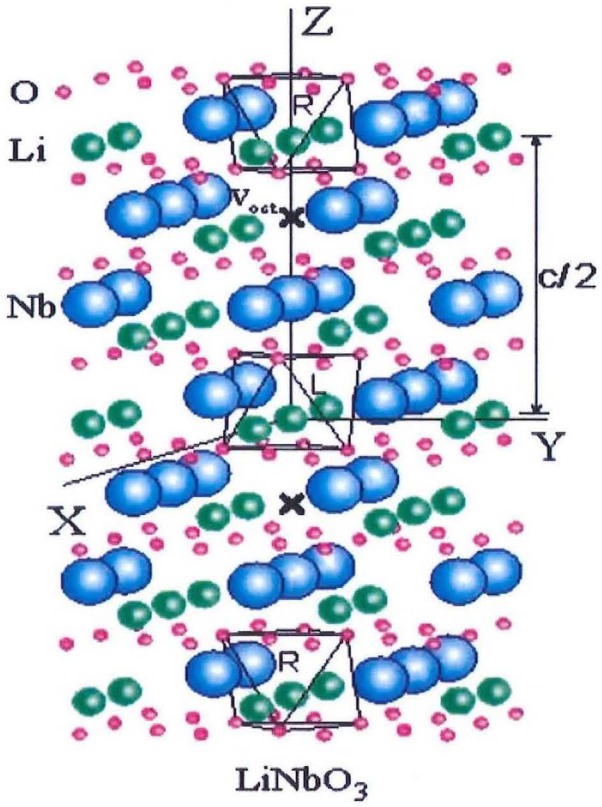

Figure 23: Lattice of ideal, defect free $LiNbO_3$ crystal [50].

In Figure 23 layers of hexagonal close packed oxygen layers (O) are visible which are interspersed with Li^+ (Li) and Nb^{5+} (Nb) ions. $LiNbO_3$ belongs to the trigonal space group R_{3c} and has permanent electric dipoles, hence the piezoelectric effect. V_{oct} denotes octahedral vacancies.

4.1 Design of 180 MHz SAW devices

4.1.1 Design considerations

For a detailed introduction of the design rules refer to section 1.1.

Table 6: Design of 180 MHz SAW devices.

Substrate material	$LiNbO_3$, 128 ° RY cut
Metal for IDTs	Aluminium or Gold on NiCr
Mechanical dimension (boundary conditions)	Max. structure size (window of reticle): 6 x 6 mm Min. structure size (manufacturing using optical lithography): 2 μm
Phase velocity of sound, v_s	$LiNbO_3$: 3600 m/s (surface acoustic wave)
Center frequency, f_{RES}	180 MHz
Acoustic wavelength, λ	20 μm $\quad (\lambda = \frac{v_s}{f_{RES}})$
Aperture, a (ID tags)	50 λ (design rule)
Number of interdigital fingers, n SAW oscillators SAW ID tags	 n = 500 (chosen) n = 50 (design rule)
Metallisation thickness, h	$\approx$ 50 nm

SAW resonator

This resonator is designed as a one-port resonator (synchronous resonator).

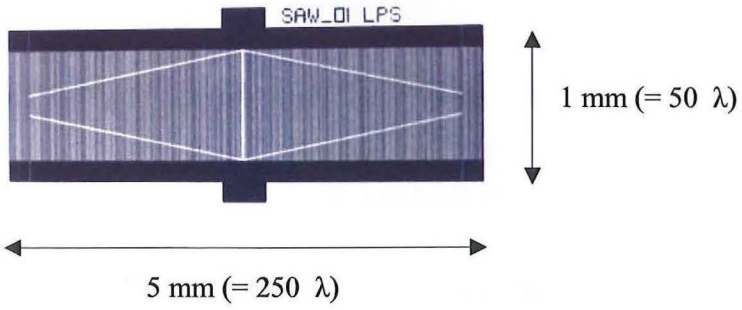

Figure 24: Design of SAW resonator using L-Edit.

The solid black areas in Figure 24 are conductive tracks connecting the IDT with the wire bonding pads. The grey hatched areas represent the IDT and are in fact lot of fine lines. The SAW resonator was designed with 500 interdigital fingers, using the maximum possible design size. Note: Due to the limited resolution of the picture the design does not show clearly.

SAW ID tags

SAW ID tags are designed as one-port resonators too. Four individual patterns were designed, reproducing a 2 bit code. The two reflectors represent one bit of information each.

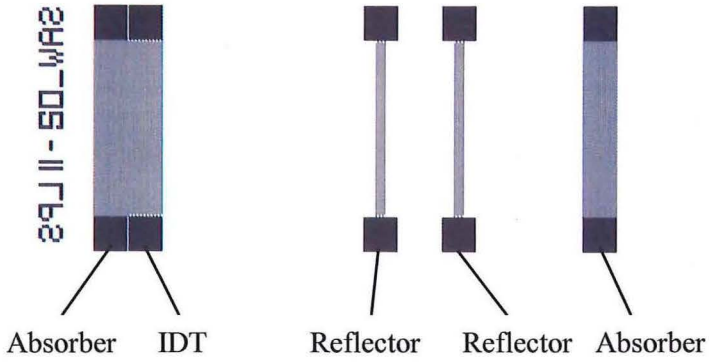

Figure 25: Design of SAW ID tag.

Figure 25 shows the arrangement of the SAW ID tag. The solid black areas are wire bonding pads and the grey areas IDT/reflectors/absorbers, consisting of fine lines. Note: Due to limits in resolution the fine lines appear grey.

4.1.2 Fabrication of SAW devices

1. Manufacturing of SAW structures involve using photolithographic processes to define the SAW pattern after Au metal evaporation and spinning of photo resist and wet etching of Au to form the SAW structure.
2. On-wafer test of SAW structures to detect shorts in IDTs and to determine resistance of conductive tracks to find defect-free devices.
3. Cutting out of individual defect-free devices with a diamond saw.
4. Wire bonding to PCB using Al wire
5. Fitting of wires to PCB and tuning as $\lambda/2$ antenna

Figure 26: Two SAW ID tags during fabrication.

Figure 26 shows two different ID tags after cutting out of the substrate. One contains one reflector, the other two reflectors. Note: Due to the size of the devices it was not possible to get any better quality pictures.

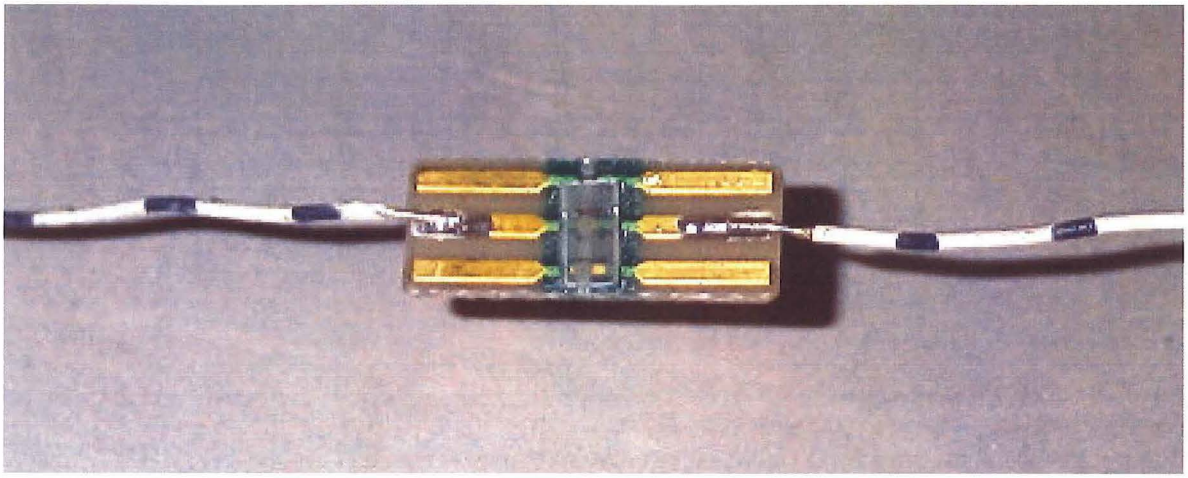

Figure 27: SAW ID tag (visible in center) connected to antenna.

Figure 27 shows a SAW ID tag mounted on a small PC board (contact strip). The connections to the IDT are made with wire bonding. The antenna is soldered on to the pads.

4.1.3 Testing and results

The testing of the devices was done using the setup as of section 3.2.

Results for SAW resonator

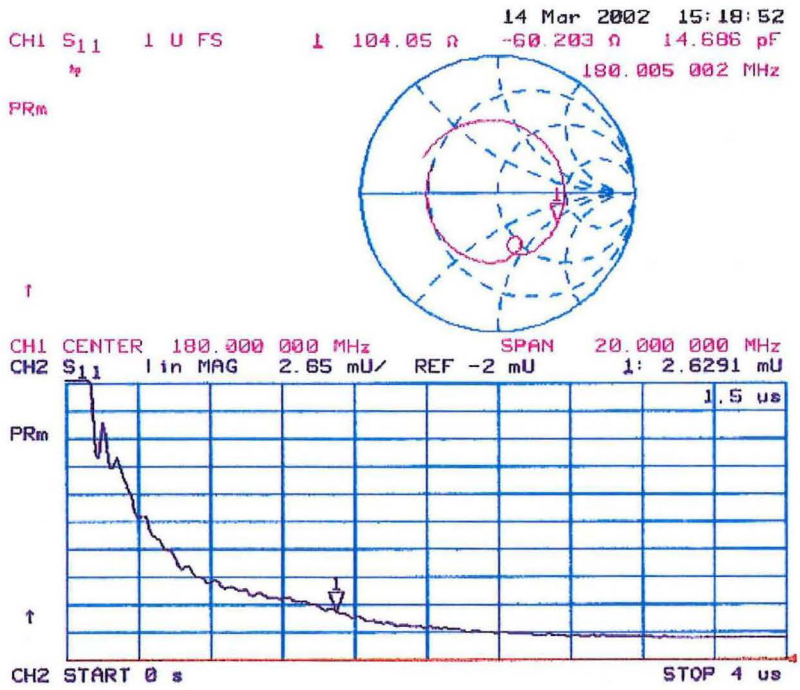

Figure 28: Reflections measured off SAW resonator.

In Figure 28 CH1 shows in a Smith chart the oscillating response signal at around 178 MHz, against a theoretical 180 MHz. CH2 shows the signal sent back from the SAW resonator. The signal decays over a time of around 2 μs. It is the inverse Fourier transformed spectrum, measured on the antenna.

The measured oscillation frequency is slightly below the designed value (about 1% off). This might be caused be the electrical load of the antenna and mass loading or inaccuracies during the fabrication. A fine-tuning is possible by slightly changing the acoustic wavelength λ or by using an external tuning circuit.

With these measurements the quality factor and the bandwidth of the oscillator can be determined approximatively.

The quality factor Q is given as

$Q \approx \varpi * \tau$ (valid for $Q >> 1$), $\varpi = 2 * \pi * f_{Res}$

where f_{Res} is the measured oscillating frequency of the SAW resonator and τ is the time it takes for the signal to decay to 63% of its end value (as of Figure 28, τ is around 800 ns).

$$Q = 2 * \pi * 178MHz * 800ns = 895$$

The quality factor is defined as follows $Q = \frac{f}{\Delta f}$

where Δf is the bandwidth of the oscillator

The bandwidth is therefore $\Delta f = \frac{f}{Q} = \frac{178MHz}{895} = 199kHz$

This is an oscillator with notable technical characteristic, considered that the design has not been optimised.

Results for SAW ID tags

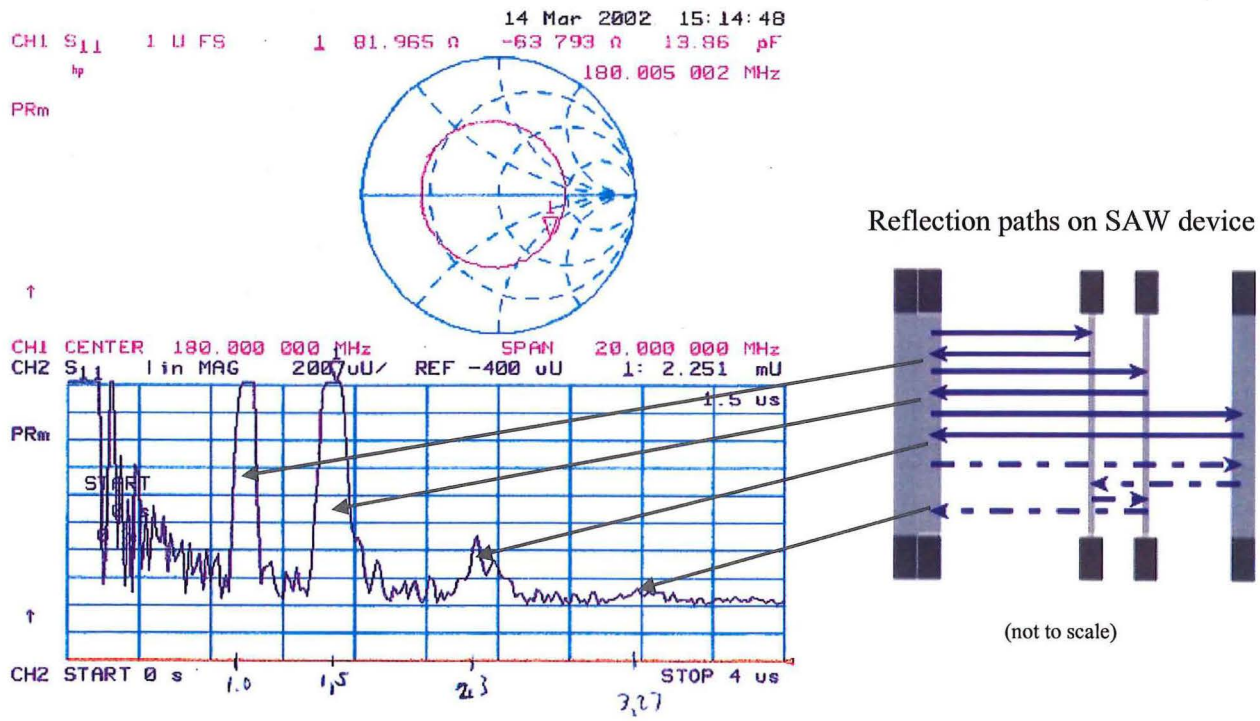

Figure 29: Reflections measured off 180 MHz SAW device with two reflectors.

Figure 29 is a graph taken from the network analyser. It is the inverse Fourier transformed spectrum, measured on the antenna, coming back from the SAW device (Figure 25). It shows several peaks at

around 1 μs, 1.5 μs, 2.3 μs, and 3.27 μs. These represent the two reflectors, the absorber (the absorber acts as weak reflector as well), and a very weak multi path reflection. The first two reflections at 1 μs and 1.5 μs have a large amplitude which allows an interrogation over considerable distance. In other words, the received signal has a high signal-to-noise ratio.

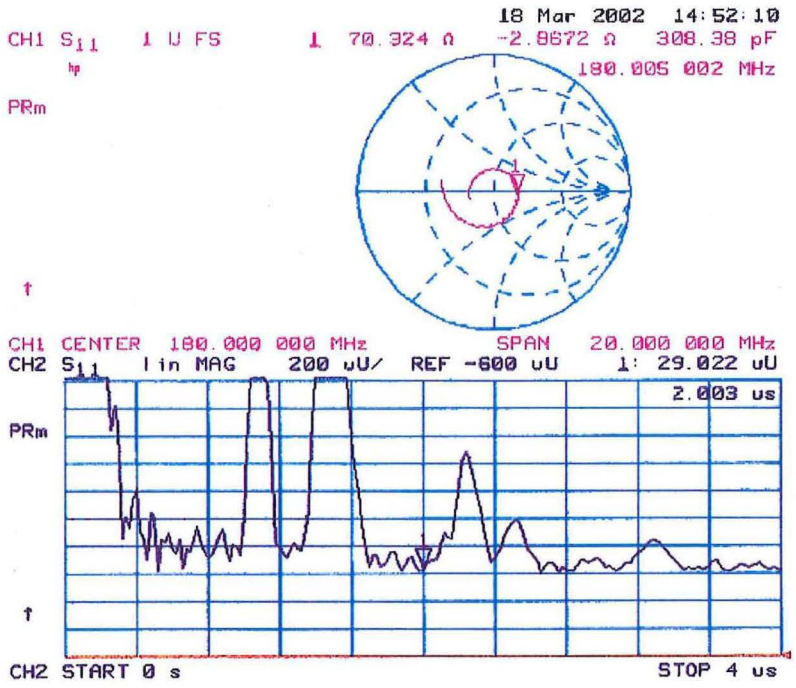

Figure 30: Reflections measured off another 180 MHz SAW device with two reflectors.

Figure 30 is a graph taken from the network analyser. It is the inverse Fourier transformed spectrum, measured on the antenna, coming back from the SAW device. It shows several peaks at around 1.1 μs, 1.5 μs, 2.25 μs, and 2.55 μs. Again, the received signal has a high signal-to-noise ratio. Compared to Figure 29, the measured delay times are slightly different which might be caused by fabrication tolerances.

4.1.4 Calculation of phase velocity

With the measurements obtained from Figure 28:

$$v_s = \lambda * f_{RES} = 20\mu m * 178MHz = 3560\frac{m}{s}$$

This is very close to the theoretical figure of $3600\frac{m}{s}$.

4.1.5 Influence of temperature

The piezoelectric properties of most commercially used substrate materials are temperature dependent (see Table 2). This has an influence on the measured results.

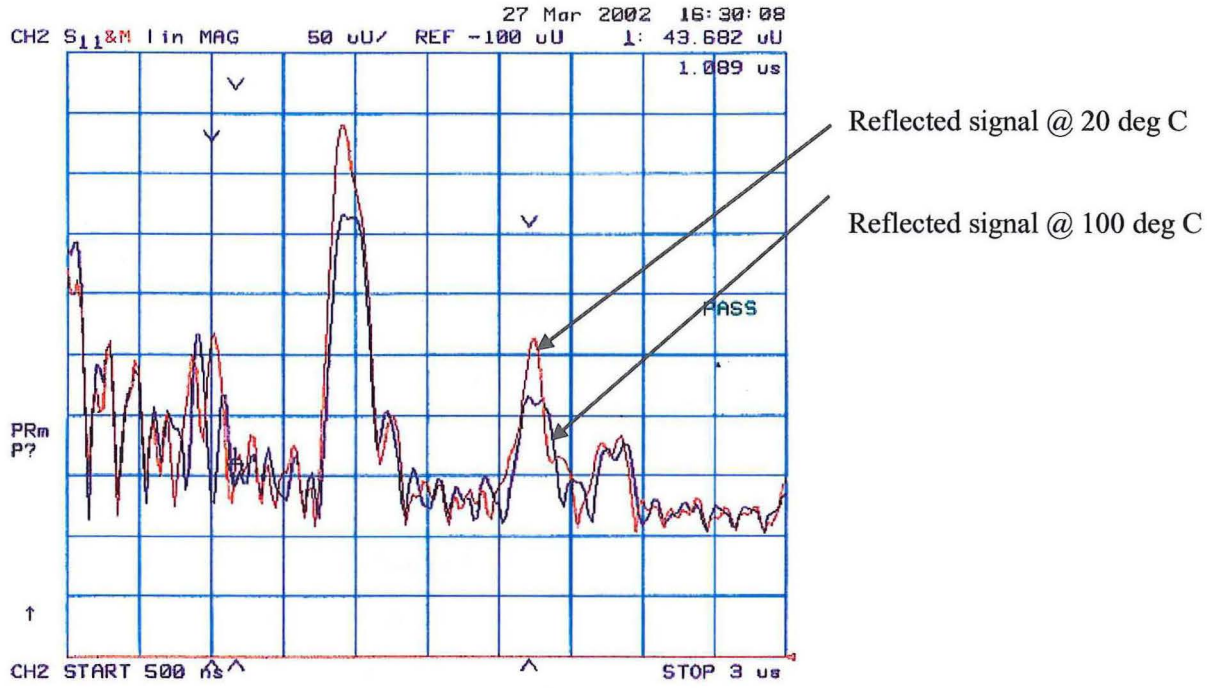

Figure 31: Influence of changing temperature on $LiNbO_3$ substrate.

As recorded in Figure 31, the reflected signal is weaker at elevated temperature than at room temperature, which would lead to a decrease in read-range. Also, if a value is transmitted via modulating the amplitude of a reflected peak, this value will be influenced by temperature.

4.1.6 Trials to measure strain

A SAW ID tag was connected to an antenna as of Figure 27, but only suspended on the two sides (at the position of absorbers). Like this, the substrate maybe bent downwards when a force is applied in the centre. The substrate would receive compression on the upper side and tension on the lower side, divided by the neutral phase (flexible deformation).

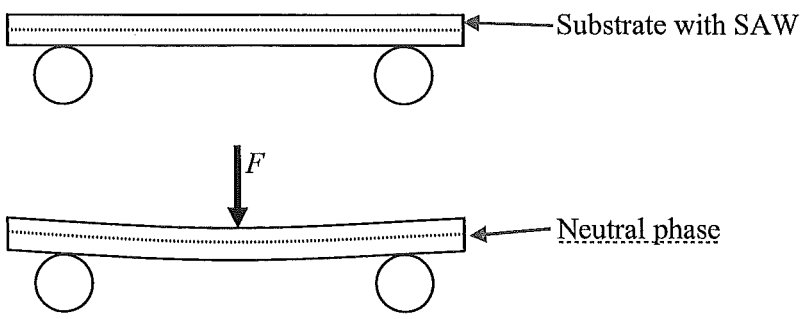

Figure 32: SAW device on two support strips as set up to measure strain

A SAW device was suspended on two support strips as shown in Figure 32. A force was applied in the centre of the sample and the reflected signal analysed. No change in signal was evident but on the second attempt the SAW ID tag was destroyed. The conclusion is that $LiNbO_3$ in the present form is unsuitable for strain measurement, possibly due to the excessive thickness of the substrate. Literature search revealed no references in this area either.

4.1.7 Findings

The analysed SAW devices produced very strong reflections and a good wireless range of up to 2.5 metres was observed (using setup as of section 3.2). A low yield on the produced wafers (< 20%) might be caused by deposits on the substrate and a poor cleaning regime. The metal coating on the substrate is not abrasion resistant and the handling can lead to abrasion of the metal which will compromise the performance. The thickness of the metal deposition (SAW structure) has an influence on the strength of the reflections, a quite big difference between various SAW devices was observed (see section 1.3).

4.2 Design of 360 MHz SAW devices

Some more SAW devices were fabricated in a higher frequency range. The aims were to demonstrate fabrication of microelectronic structures at the limits of our optical lithography tools and to learn about the range of the wireless communication at higher frequency. These SAW devices are based on the same designs as described in section 4.1, except that the design was reduced to half size by a shrinking factor while exposing the photomask.

Outcome

A couple of working devices were fabricated. Subsequently the SAW devices were measured (as of section 3.2). The wireless range was more than 2 meters and the same as experienced with the 180 MHz devices.

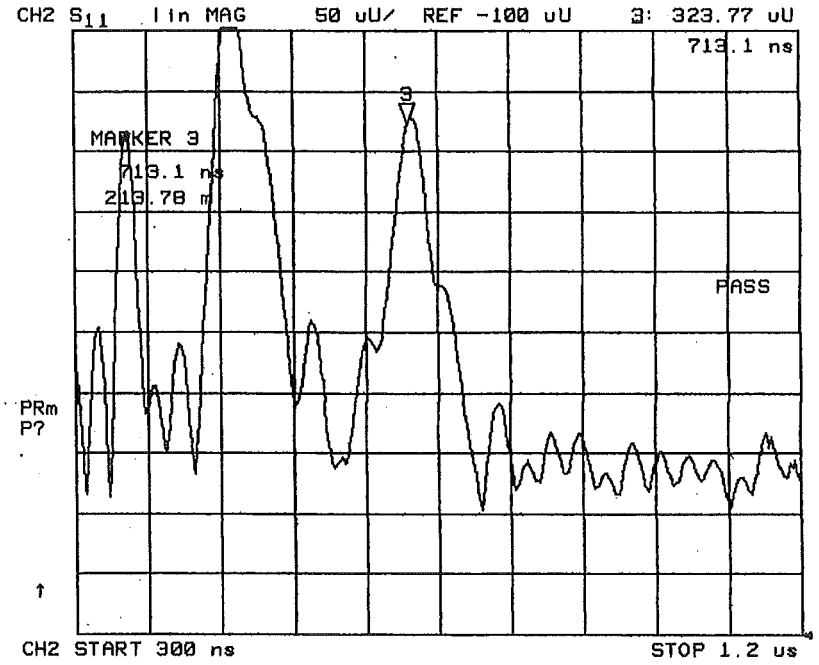

Figure 33: Reflections measured off 360 MHz SAW device with two reflectors

The reflected signal off a SAW ID tag as shown in Figure 33 has two distinct reflections at around 490 ns and 720 ns. It is recorded off an ID tag with two reflectors and one absorber (as shown in Figure 29) and the delay times were half of the ones recorded there. This was expected as the physical size is shrunk to half compared with the 180 MHz SAW ID tag. The smaller reflection at around 360 ns could be caused be a stray reflection.

4.3 Design of 2450 MHz SAW devices

A couple of constraints dictate the use of even higher frequency SAW devices to measure strain.

- Working frequency should be in an Industrial, Scientific and Medical radio band (ISM) to facilitate worldwide use
- Space constraints on mechanical parts to be measured require a small circuit footprint
- Size of antenna needs to be minimised so it can be accommodated in the confined area

Reports about SAW devices working up to 10 GHz [19-21] suggests no fundamental limit in upper frequency of SAW devices, beyond limits in lithography.

Due to the resulting small pitch in the submicron range, EB lithography or evanescent near field [51-54] lithography has to be used. It is feasible to utilise Nano Imprint Lithography (NIL), which would lead to higher throughput [55, 56].

For these trials, the Philips EBL system was originally used (this EBL system has since been replaced by a state of the art Raith 150 EBL system). For more information about EBL refer to section 2.4.

4.3.1 Design considerations

EBL lithography has its own limitations with regards to feature size and maximum write field size. The Philips EBL system, used for this research, is basically a SEM system with an added tracking generator. It can expose 4096 by 4096 Pixels in one write field. Joining write fields is not a viable option.

The following table shows the relationship between pixel size and write field size on the Philips EBL system (only low magnifications shown).

Table 7: Write field sizes and pixel sizes for the Philips EBL system.

Magni-fication	X Write field	Y Write field	X Pixel Size	Y Pixel Size
	(µm)	(µm)	(µm)	(µm)
40	3514.85	2247.52	858.1	548.7
80	1645.54	1124	401.7	274
160	868.69	604.04	212.1	147.5
320	434.57	296.3	106.1	72.3
640	222.22	153.09	54.3	37.4

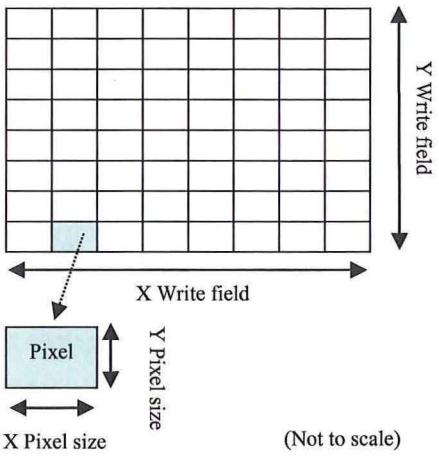

Basically, a magnification has to be chosen which will both accommodate the smallest features and the overall size of the design.

Table 8: Design of 2450 MHz SAW device.

Substrate material	$LiNbO_3$, 128° RY cut
Metal for IDTs	Aluminium or Gold on NiCr
Mechanical dimension (boundary conditions of Philips EBL system)	Max. structure size: Depending on resolution Min. structure size: Depending on resolution Size of contact pads (wire bonding): minimum 100 x 200 μm
Phase velocity of sound, v_s	$LiNbO_3$: 3600 m/s (surface acoustic wave)
Center frequency, f_{RES}	2450 MHz
Theoretical acoustic wavelength, λ	1.469 μm $\quad (\lambda = \frac{v_s}{f_{RES}})$
Chosen acoustic wavelength, λ	1.446 μm = 4 * 361.5 nm (361.5 nm = 5 pixels in y direction for 320 times magnification)
Number of interdigital fingers, n	n = 50 (design rule)
Metallisation thickness, h	≈ 50 nm

It is obvious that the chosen λ will lead to an increase of the center frequency. But it is also reasonable to infer that the actual center frequency will be slightly off the designed frequency (see section 4.1.3).

The chosen magnification of 320 offers a good approximation to the wanted wavelength and also allows the design (IDT plus wire bonding pads) as a whole to be written.

Due to these constrains, the Philips EBL system can only write one IDT, reflector or absorber with wire bonding pads per exposure. The sample needs to be repositioned manually before writing the next structure.

The exposure time was around one hour (dependent of the feature size, complexity, and the dosage, which was generally set to 600μC/cm^2). The devices were fabricated as illustrated in 2.4.

Several patterns were fabricated and are discussed below:

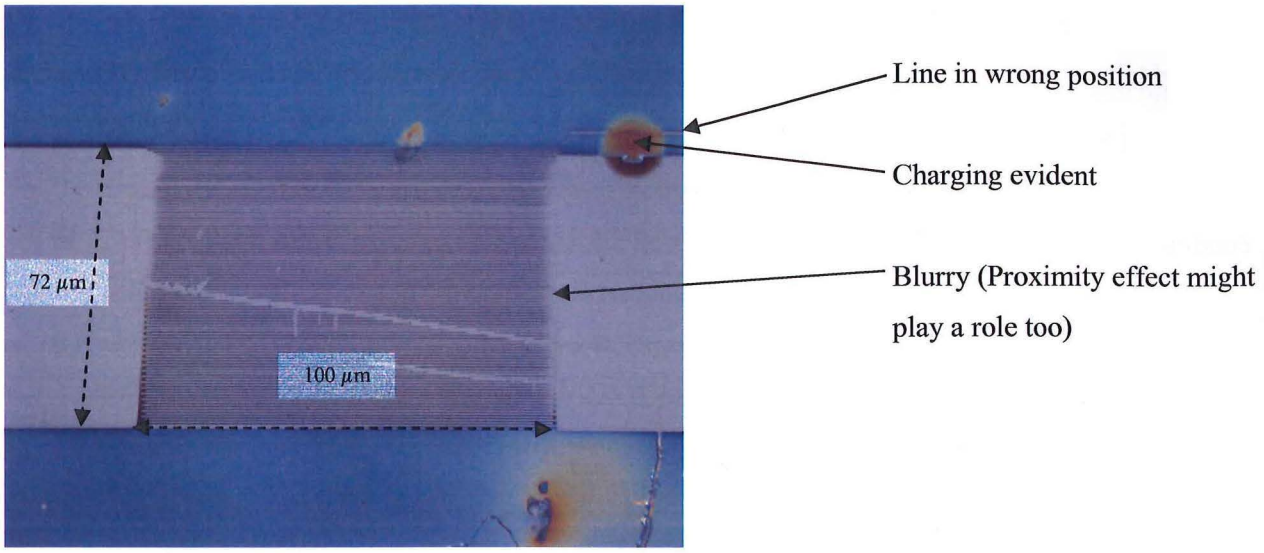

Figure 34: Optical microscope image showing imperfect SAW IDT on $LiNbO_3$.

Figure 34 shows several problems:

- Lines in wrong position or missing
- Charging evident
- Blurry picture

The $LiNbO_3$ substrate used is highly insulating, piezoelectric, and pyroelectric; a charge will build up during exposure which can lead to undesired effects. The beam strays away and the exposure is not as accurate as expected. Also it is evident that the pattern generator has frequent malfunctions, leading to missing exposure areas (one or several lines not exposed).

In order to circumvent these well known phenomena, different approaches were trialled to overcome the charging problems: A conductive polymer was trialled, a gold layer for charge dissipation was evaporated over the PMMA and a wafer was chemically reduced. These methods are described in section 2.9.

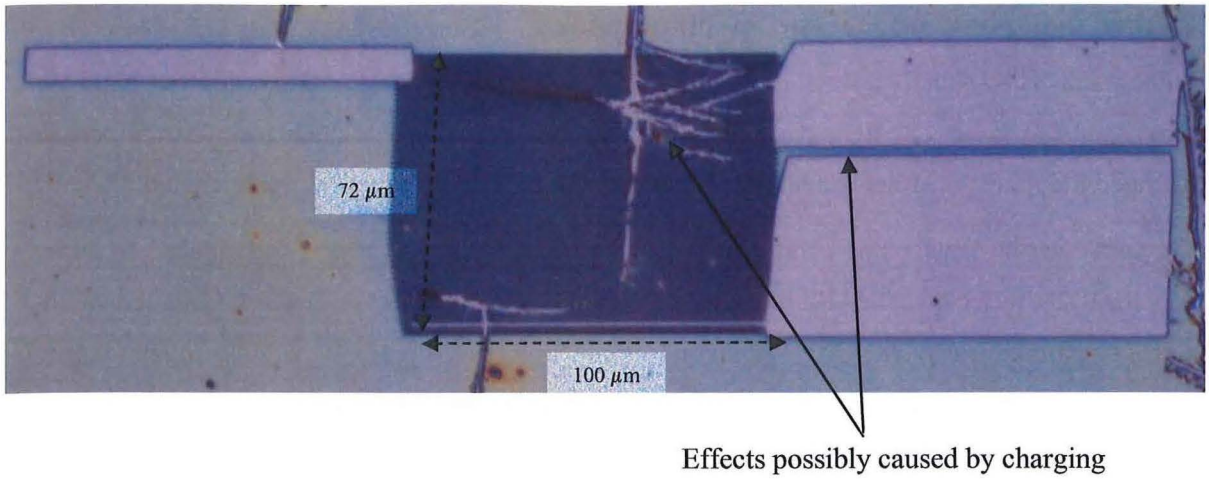

Figure 35: Optical microscope image showing another imperfect EBL exposure.

Figure 35 shows again the effect of missing exposure lines and charging. In the center of the picture there is an area that looks like scratches, but this is possibly caused by charging. The area with the missing exposure lines on the right hand side might have been caused by to a sudden discharge and the associated realignment of the electron beam.

Figure 36: Optical microscope image showing Multiple EBL exposures

Figure 36 shows multiple exposures (dimensions as of Figure 35). Three identical exposures were made with a translation along the x-axis between the exposures. One problem encountered was that the three exposures were out of alignment which would lead to weak or no reflection of the SAW signal. The other problems were that some lines were missing (the electron beam was blanked in these areas for some reasons).

The system does not seem to allow the alignment of multiple exposures. It is obvious that poorly aligned IDTs and reflectors would not yield good return signals. Therefore, an attempt was made, to use optical lithography for the wire bonding pads, followed by EBL for the fine lines of the IDT. This should also allow easier alignment for multiple exposures.

4.3.2 Trials using both optical and EB lithography

EBL lithography is essentially a serial process and is slow, especially if larger areas (i.e. wire bonding pads) have to be exposed. The EBL system has severe stability problems (instable beam current, crashes) as illustrated in Figure 35. A new attempt was made, to circumvent the problems encountered.

A photo mask was designed using L-Edit with several wire bonding pads strategically placed, to serve as contacts for IDTs, reflectors, and absorbers; it was manufactured at Industrial Research Limited. With substrates prepared this way, the EBL system only needed to expose the small features (350 nm lines), which takes less time and causes less charging. The contacts are also used for precise alignment of the EBL before exposure.

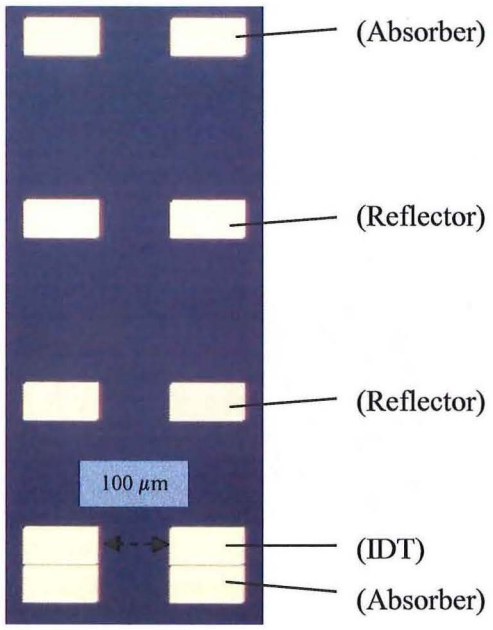

Figure 37: Optical microscope image showing fabricated wire bonding pads on $LiNbO_3$.

In Figure 37 the strategically arranged wire bonding pads are shown. The SAW structure can be fabricated at the points of interest.

After this, the sample was prepared with a bilayer of PMMA. On top of this, the sample was coated with 10 nm Au which should allow charge to dissipate. As mentioned earlier, the EBL pattern has to be precisely aligned with the Au pads. Using SEM microscopy, the two Au layers (pads plus coating for charge dissipation) are hard to separate (insufficient contrast) and the alignment is not feasible with the Philips EBL system. Another trial with an Au layer thickness of only 2 nm did not yield better visibility.

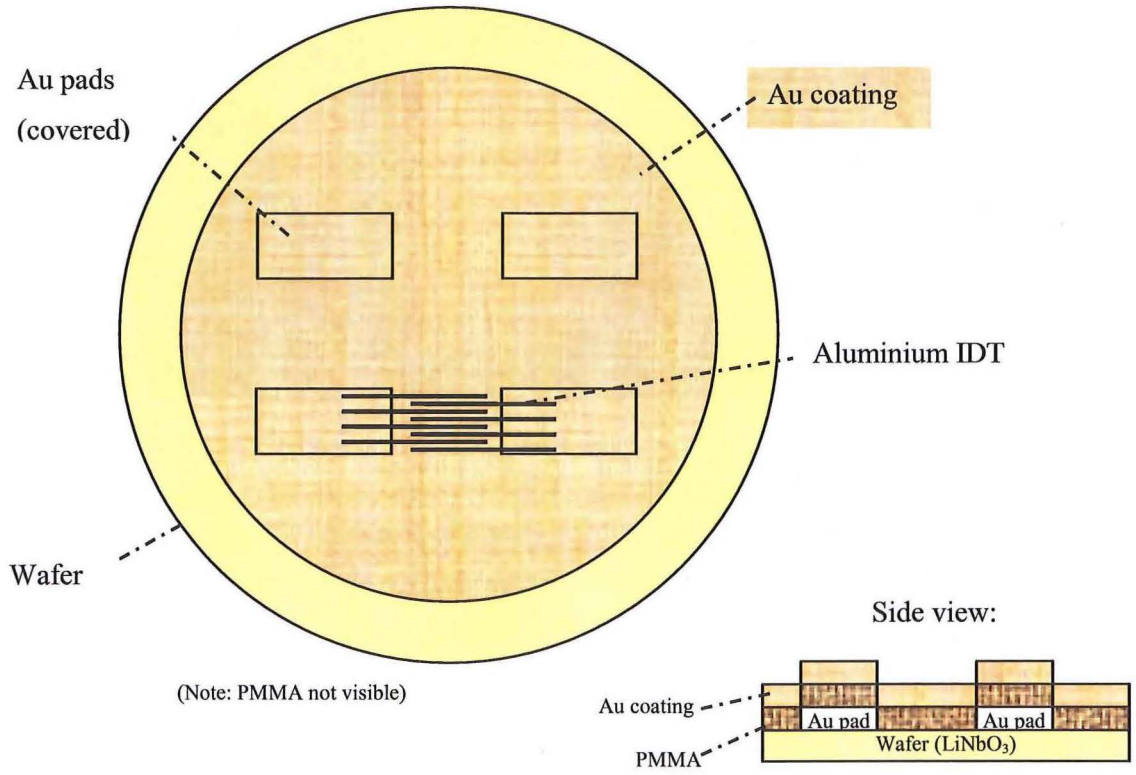

Figure 38: Schematic arrangement of Au coating for charge dissipation.

In Figure 38 the Au coating for charge dissipation is shown both in top view and side view. After the Au pads have been fabricated using optical lithography, Au evaporation and lift-off, the bilayer of PMMA is spun and baked. After this, another thin layer of Au is evaporated which will serve for charge dissipation.

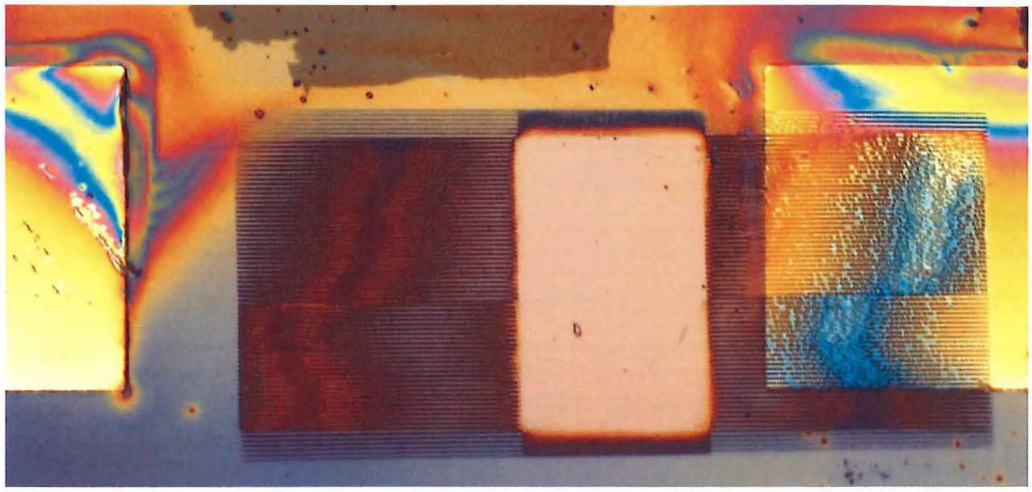

Figure 39: Optical microscope image showing EBL exposure on wafer with Au pads.

In Figure 39, discolorations (rainbow coloured) might be caused by variable PMMA thickness. The area in the center of the image is totally cleared due to overexposure and the alignment between pads and lines is poor. The exposure does not seem to be distorted and no charging problems are evident.

4.4 Summary

SAW oscillators and ID tags were successfully fabricated using optical lithography and tested with a network analyser. The prototypes with both 180 MHz and 360 MHz working frequency were successfully interrogated over a wireless range of more than 2 metres.

More SAW devices were designed for the 2450 MHz ISM band. EBL was employed due to the resulting small size of the SAW structure. $LiNbO_3$ is not only piezoelectric but also pyroelectric and both these effects lead to charging of the substrate which hampers EBL exposures. Different ways have been identified to overcome this issue.

The used EBL system does not allow a complex pattern to be written error free and alignment for exposure is not easy to achieve. Further trials were postponed as a new EBL system (Raith 150) was on order.

Chapter 5
Fabrication and characterisation of SAW devices on sputtered ZnO coatings

As reported in the preceding chapters, SAW devices were successfully fabricated and tested on $LiNbO_3$ substrates. However, $LiNbO_3$ is very brittle and therefore not a suitable substrate for measuring strain. A way had to be found, to directly apply a piezoelectric coating on a mechanical part of interest.

ZnO is a versatile material with strongly piezoelectric properties (see section 1.2.2) and has been used for this research.

ZnO coatings have been deposited using DC magnetron sputtering, characterised and optimised. However, no tests could be performed to check piezoelectricity of the ZnO. Finally, A SAW device was fabricated on sputtered ZnO on a Si wafer as base material and successfully tested which proves the piezoelectric properties of the sputtered ZnO.

SAW waves in ZnO have a higher phase velocity of sound v_s, than in $LiNbO_3$. A value of 9180m/s was reported for a SAW device on a $ZnO/SiO_2/Si$ structure [57]. Different values have been reported in [57, 58] and will need to be confirmed. The values seem to depend on the base substrate and the thickness of the sputtered ZnO.

No report of SAW devices using ZnO on stainless steel as substrate have been found but comprehensive reports of the SAW propagation in ZnO on diamond [59, 60] give an insight in this matter.

Besides that, so called interface acoustic waves (IAW), also named boundary waves, have been proposed as an alternative to classical surface acoustic waves (SAW) on a single piezoelectric substrate. IAW are propagating along the interface separating two solid bodies, one of which at least is piezoelectric [61]. This will have to be investigated in the future.

As mentioned, the rods need to be equipped with a sensing structure. A rod is a structure made of stainless steel, with a nickel coating. Only one flat area on the rod is suitable for optical or EB lithography.

For this work, the Raith 150 EBL system was used. This EBL system has a stitch field size (size of one exposure field) of 100 by 100 µm but can perform automatically stitching for larger designs.

5.1 Preliminary Trials

The first rods were sputter coated at RMIT (Royal Melbourne Institute of Technology). RMIT have a long track record in this area. The following SEM and AFM images were taken in our lab.

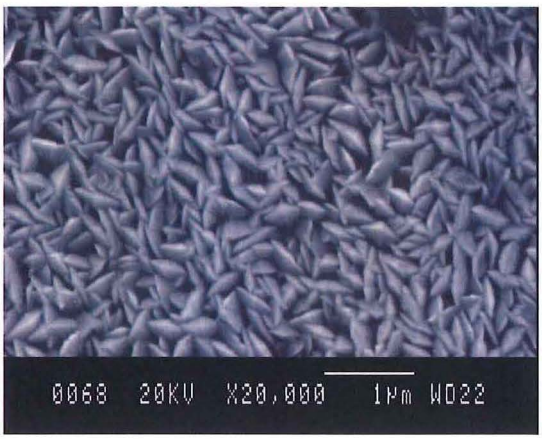

Figure 40: SEM image of sputtered ZnO on rod showing microstructure (top view).

Figure 40 shows the microstructure of the individual ZnO grains. The size of the individual microstructures is in the area of 100 to 250 nm.

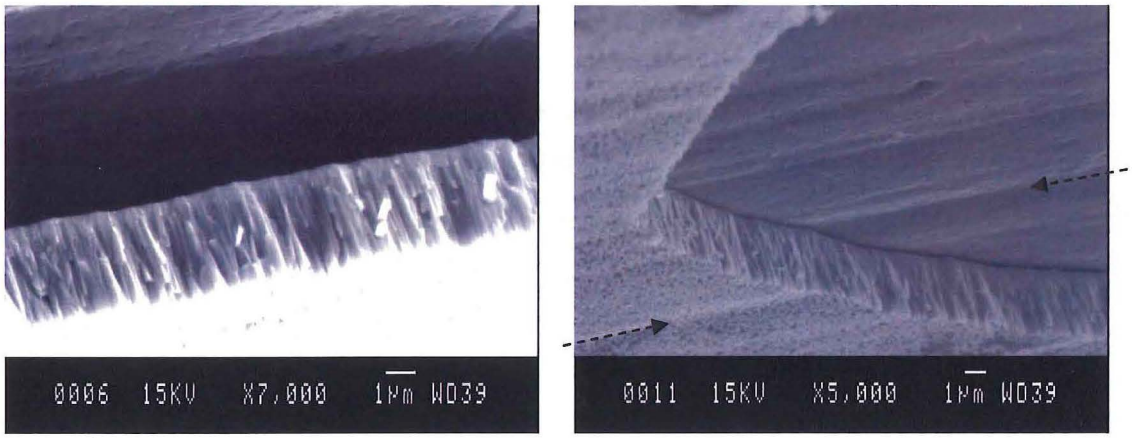

(a) (b)

Figure 41: SEM images of sputtered ZnO on rod showing microstructure (side view).

In Figure 41 (a) and (b) crystal growth is easily visible. The thickness of the coating is around 3 μm. The individual crystals are oriented normal to the surface. Scratches in the surface as visible in (b) are still visible on top of the sputtered layer, this indicates that ZnO does not seem to smooth out the surface.

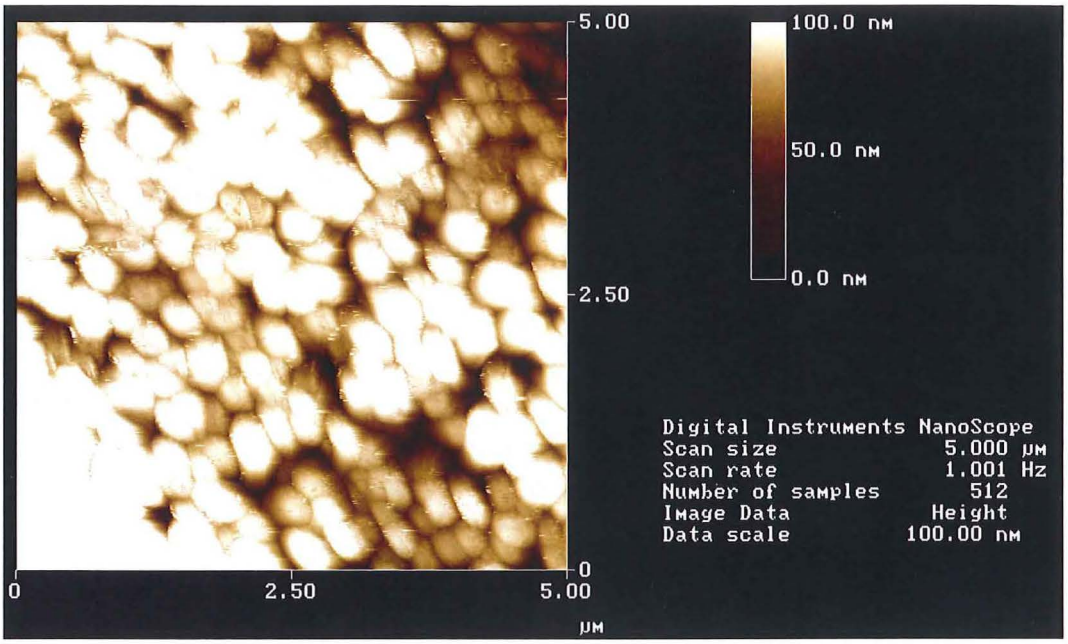

Figure 42: AFM scan in tapping mode shows grains of sputtered ZnO (top view).

Figure 42 shows deep depressions as dark spots (> 100 nm) on the scanned area. The size of the beads appears as around 500 nm. Note: This scan could not be repeated as the sample was sent away for other trials.

More investigations are needed to improve the quality of the surface finish on the rod.

5.2 Trials In house

Later during this project a new magnetron sputtering system (Edwards Auto 500) was commissioned. For more details refer to section 2.10.3.

The following figure illustrates what parameters need to be optimised, to achieve the desired sputtering process:

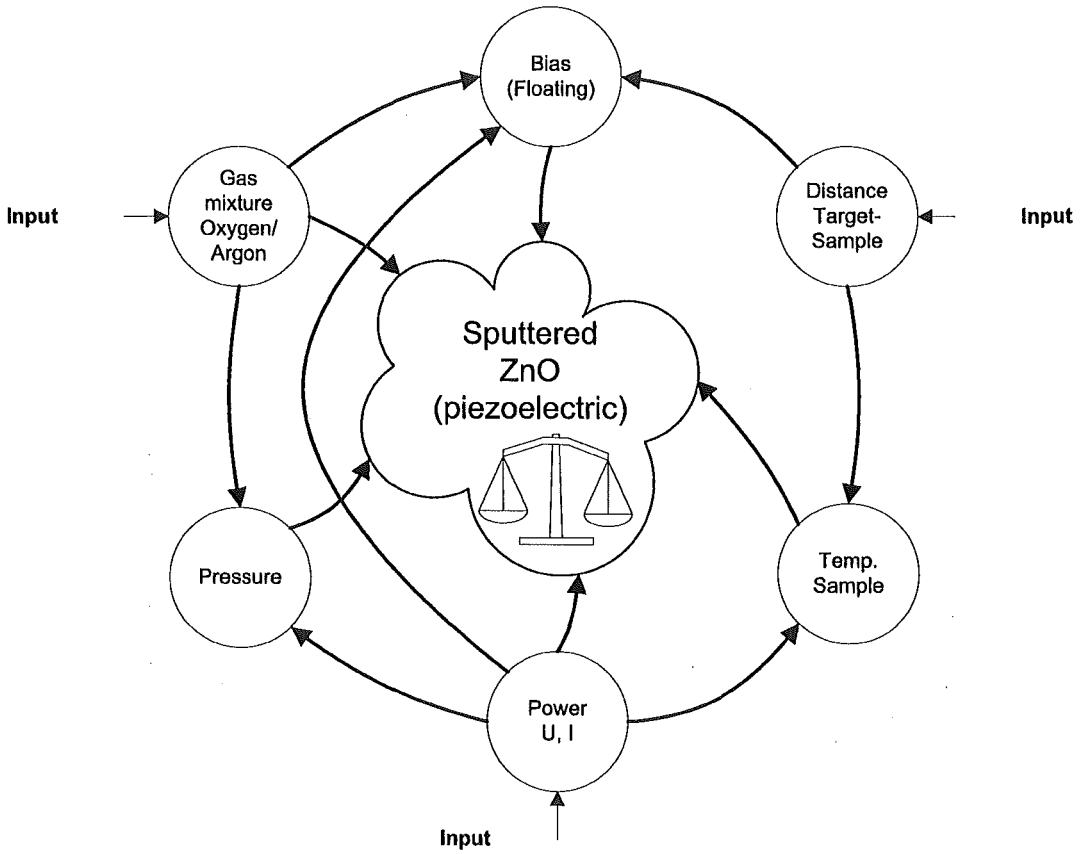

Figure 43: Relationship between various parameters during sputtering.

As shown in Figure 43, the quality of the sputtered coating depends on a set of six main parameters. Three of them can be set directly with the used system (marked as Input). One recognised approach to find the best sputtering parameters is as follows:

- Maintain process pressure constant during a series of sputtering trials
- Maintain sputtering power constant during a series of sputtering trials
- Maintain distance between target and sample constant
- Change stoichiometry by changing O_2/Ar ratio only

also:

- The sample surface is left at ambient temperature (no external heating), however the temperature will rise during sputtering
- The pressure in the vacuum chamber will rise slightly during sputtering

Preliminary trials

Many different ways are possible to sputter ZnO with the desired piezoelectric properties:

- DC magnetron sputtering
- RF magnetron sputtering
- Using Zn target and reactive sputtering (by introducing O_2)
- Using ZnO target
- Variation of pressure and distance between target and sample
- Applying of bias voltage between substrate and ground (not possible with the sputtering system used for this research)

In order to keep the trial period reasonable, a working set of parameters from [62] was used as a starting point and subsequently refined.

A set of preliminary trials with the new sputtering system where run to establish reproducible conditions and to find limits.

- The sputtering power was varied: The sputtering rate increases with power, at a power above 350 Watts sparking was observed (breakdown between target and screen around target), and the plasma was momentary lost. Therefore all future trials were done at 250 Watts.
- The distance between target and sample was set at approx. 110 mm.
- The process pressure was kept at 1.2×10^{-2} mbar for reactive sputtering (as described below)

After the preliminary trials, the sputtering procedure was defined as follows:

1. Load samples on sample holder for uniform sputtering
2. Pump down to around 10^{-5} mbar
3. Introduce O_2 (9 sccm)
4. Introduce Ar (6 sccm), or amount necessary to desired pressure of 1.2×10^{-2} mbar
5. Set up plasma source
6. Ignite plasma
7. Presputtering for five minutes
8. Sputtering to required thickness (between 250 and 500 nm)

Table 9: Sputtering trials done to optimise parameters for piezoelectricity.

O_2		Ar		Outcome (colour impression)	Sputtering rate [nm/min]	Resistance (Semiconductor Paramter Analyser)
Flow (sccm)	Partial pressure (mbar)	Flow (sccm)	Total pressure (mbar)			
5	3.4×10^{-3}	10	1.2×10^{-2}	Looks black. Dektak and AFM show rough surface.	20.0	Low resistance coating. 12.78 kΩ
7	6×10^{-3}	8	1.3×10^{-2}	Looks black. Dektak shows rough surface.	33.0	[Sample ZnO-1] Bit higher resistance than before. 29.76 kΩ
9	7×10^{-3}	6	1.1×10^{-2}	Almost transparent, rod bluish, hard to scratch	14.3	Insulator, same as glass
9	7.5×10^{-3}	6	1.2×10^{-2}	Greenish	9.0	Insulator, same as glass
9	7×10^{-3}	6	1.2×10^{-2}	Almost transparent	6.75	[Sample ZnO-2] Insulator, same as glass
11	8.5×10^{-3}	4	1.2×10^{-2}	Almost transparent	2.5	[Sample ZnO-3] Insulator, same as glass
13	1.0×10^{-2}	2	1.1×10^{-2}	Almost transparent	2.5	[Sample ZnO-4] Insulator, same as glass
9	7×10^{-3}	6	1.2×10^{-2}	Almost transparent	4.0	Insulator, same as glass
9	6.5×10^{-3}	8	1.2×10^{-2}	Almost transparent	3.88	Insulator, same as glass
9	6.5×10^{-3}	8	1.2×10^{-2}	Almost transparent	6.63	Insulator, same as glass
9	6.5×10^{-3}	8	1.1×10^{-2}	Almost transparent	6.6	Insulator, same as glass
9	6.5×10^{-3}	8	1.3×10^{-2}	Almost transparent	5.68	[Sample ZnO-5] Insulator, same as glass
9	6×10^{-3}	9	1.2×10^{-2}	Purple	6.3	Insulator, same as glass

Note: [Sample ZnO-1 to ZnO-5] have been tested with RBS, see section 5.3. Sample ZnO-2 had the best stoichiometry.

Outcome:

- The optimal ZnO is highly translucent (transparent) to the eye.
- The resistance of the optimal ZnO is very high (measured value the same as that of the glass substrate).
- Typically achieved sputtering rates in the ZnO mode are between 5 and 10 nm per minute for the given parameters.

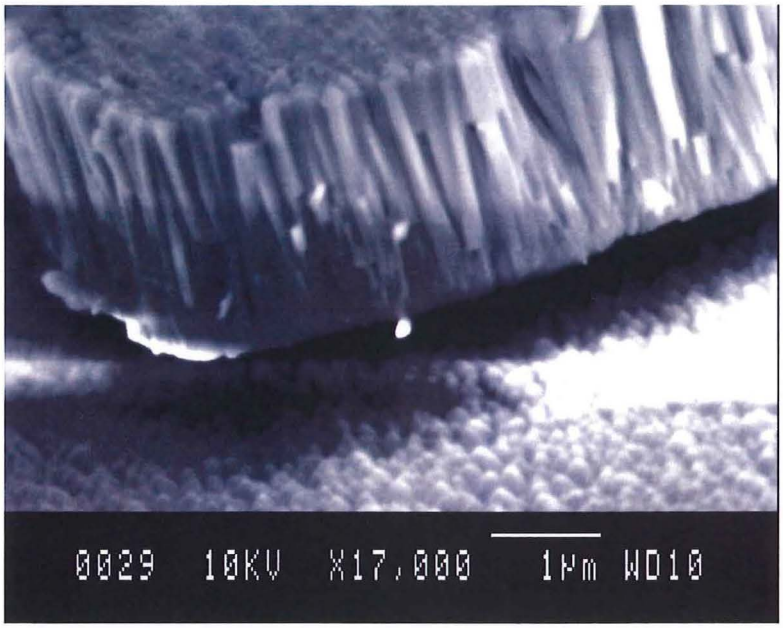

Figure 44: SEM image of sputtered ZnO showing dense polycrystalline growth.

Figure 44 shows the surface of the sputtered ZnO and a "floating" piece on top, which broke off. The individual crystals are well developed. This is an image of sample [ZnO-2]. The thickness of the sputtered ZnO looks around 2 μm rather than the planned 500 nm. The crystal thickness monitor was recalibrated after these measurements.

Problems

If the plasma is started with O_2 only (presputtering as suggested in [62]) and Ar introduced later, Zn will be deposited rather than ZnO (characterised by much higher sputtering rate, dark colour and low resistance).

Another problem was inaccurate reading of the vacuum in the chamber due to drifting of the vacuum gauges which made it difficult to get the right stoichiometry. A residual gas analyser (Quadropule unit) would enable a more accurate control of the process for more consistent results.

5.3 Influence of the oxygen partial pressure

The gas composition acts in the following ways on the resulting film:

- Changing the oxygen partial pressure during sputtering directly influences the oxidation level of the resulting film (see results in Table 10).
- The sputtering rate changes with the oxygen partial pressure. A range of around 4 to more than 30 nm/min was observed. Generally, a low sputtering rate is observed at the proper stoichiometry.

The following Rutherford backscattering scan results confirmed the good stoichiometry of the samples ZnO-2 and ZnO-3.

Table 10: Detailed RBS results of ZnO films deposited on glass.

Film	Thickness (nm) *	Composition (at.%) ± 1%	Zn/O ratio	Surface roughness (estimate)	uniformity	Thickness of oxygen rich layer at surface (nm)
ZnO-1	160 ± 20,	Zn= 63% O=36%	1.75	≈30 nm	Ok	10 ± 5
ZnO-2	315 ± 20,	Zn= 50% O=49%	1.02	≈50 nm	Ok	20 ± 5
ZnO-3	220 ± 20,	Zn= 52% O=48%	1.08	≈30 nm	Ok	10 ± 5
ZnO-4	160 ± 20,	Zn= 53% O=46%	1.15	≈30 nm	Ok	10 ± 5
ZnO-5	50 ± 10,	Zn= 42% O=56%	0.75	≈20 nm	Ok	N/A

* ZnO thickness based on density as 5.6 g/cm^{-3}

Note: Sputtering parameters can be found in Table 9.

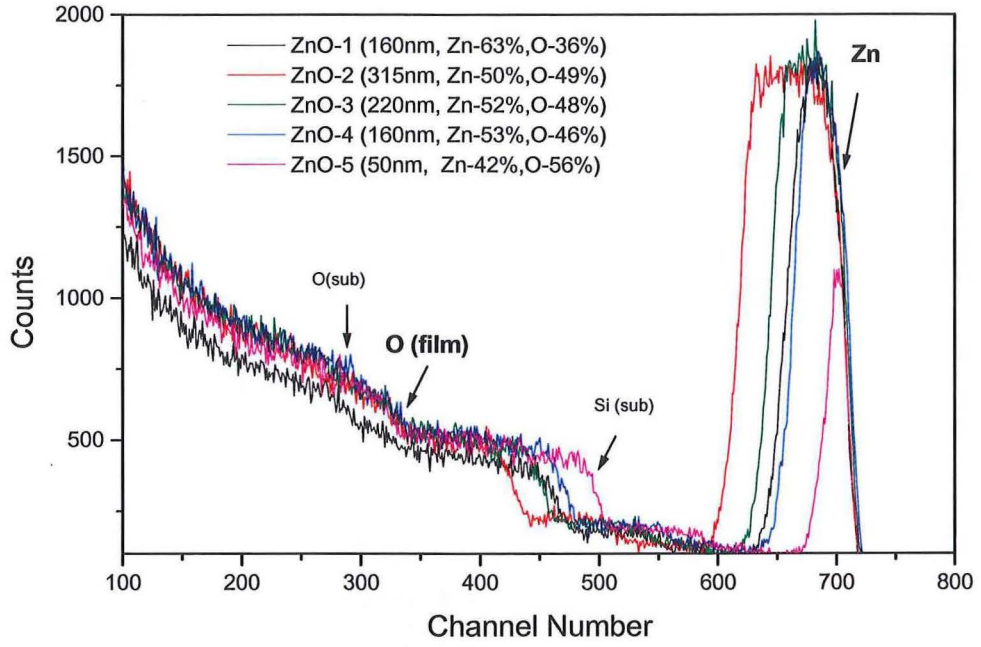

Figure 45: RBS spectra of ZnO film deposited on glass.

In Figure 45 the graphs of the five measured samples (Table 10) are shown. The steps shown in the channel area just under 300 are O peaks of the substrate and the steps shown in the channel area from 420 to 500 are Si peaks, measured from the base material (SiO glass slider). The steps shown in the channel area of around 320 are O peaks measured from the film. The peaks shown in the channel area from 600 to 700 are Zn peaks and the width of the peak is a measure of the thickness of the coating.

5.4 X-ray diffraction results

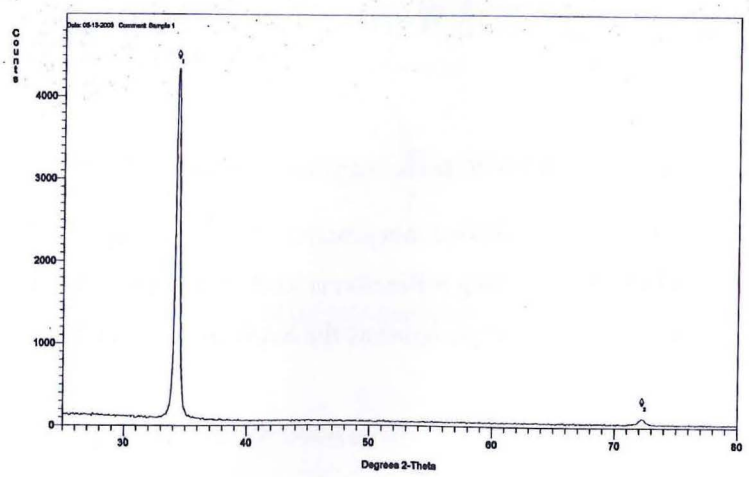

Figure 46: X-ray scan of sample ZnO-2.

The first peak detected in Figure 46 is located at 34.287 deg (d-space = 2.615) which represents [002] growth of ZnO and the second peak is located at 72.22 deg (d-space = 1.308) which represents [006] growth of ZnO (which is parallel to [002] growth).

Compared with the results of "norm" ZnO samples (using database) the results in Figure 46 show a strong correlation with polycrystalline ZnO with preferred growth in 002 direction.

5.5 SAW device on Si wafer

Some SAW devices were fabricated on sputtered ZnO to prove that the coating is in fact piezoelectric. ZnO was sputtered on a Si wafer and the pattern defined using optical lithography.

S 1813 photo resist was spun on the coated n-type Si wafer and exposed using a mask containing SAW structures (mask of 360 MHz SAW design as of section 4.2). After developing it was cleaned using the oxygen plasma asher to remove residual resist. 200 nm of Al was deposited using thermal evaporation, followed by lift-off (as described in section 2.3). The designs were inspected using optical microscope and resistance measurement. Two SAW devices were successfully tested using the set up as of section 3.2 but using a direct wire connection to the SAW device.

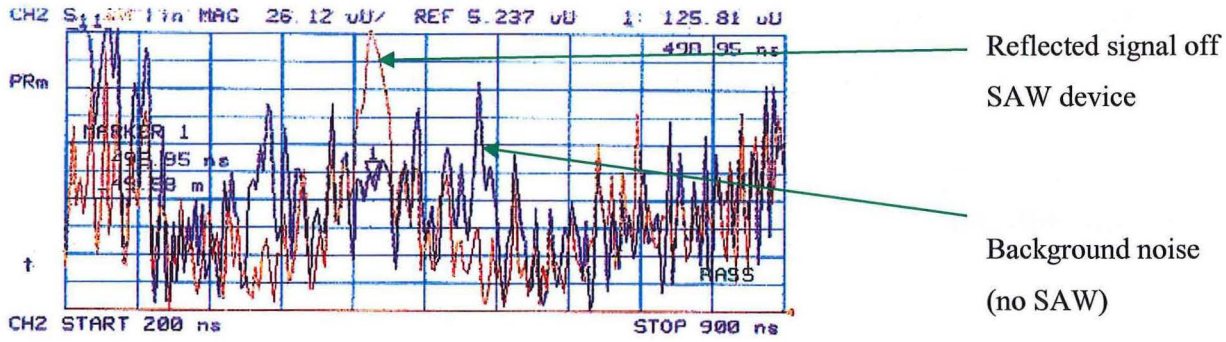

Figure 47: Reflections measured off SAW device on ZnO and Si.

In Figure 47 the reflections off the SAW device fabricated on ZnO are shown. The oscillating frequency was determined at around 430 MHz. A strong reflection is visible at around 500 ns. This graph cannot easily be compared with the results of other samples as the SAW device was interrogated while still on a wafer and using a wired connection.

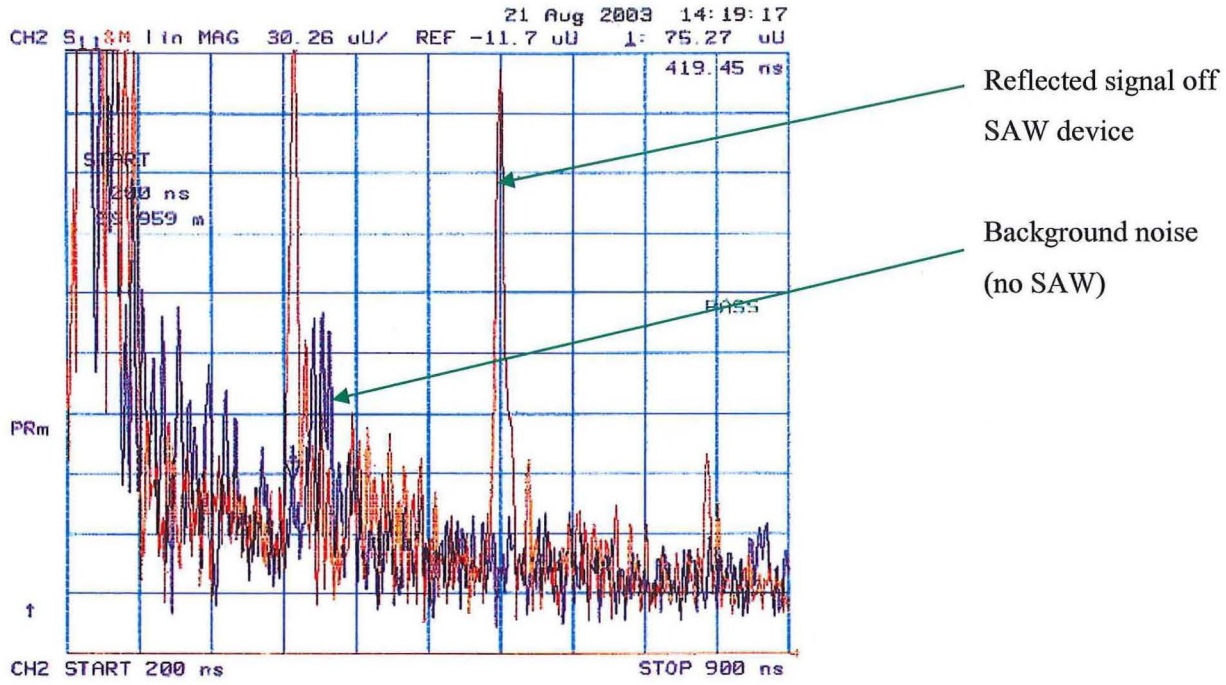

Figure 48: Reflections measured off another SAW device on ZnO and Si.

Figure 48 shows the reflected signal of another SAW device. Two strong reflections are visible at around 420 ns and 620 ns.

With the information gathered of these SAW devices the phase velocity of ZnO on Si can be determined.

Thickness of sputtered ZnO 600 nm

Thickness of evaporated Al 180 nm

Oscillation frequency, f_{RES} 430 MHz

Acoustic wavelength, λ 10 µm $(\lambda = \frac{v_s}{f_{RES}})$

Phase velocity of sound, v_s $v_s = \lambda * f_{RES} = 4300 \frac{m}{s}$

The phase velocity is much lower than the 9180 m/s expected [57]. This issue will need to be investigated further.

Another task to be performed is the determination of the dielectricity.

5.6 SAW devices on stainless steel rods

For ease of manufacturing it is desirable to add the SAW structure directly on the mechanical parts to be measured, without any additional steps such as polishing. However, preliminary trials showed that the surface finish is not good enough as a base for the SAW structure. Therefore, several rods were manually polished and sputter coated with ZnO (for information on sputtering refer to section 2.10.2). A bilayer of PMMA was spun and the design fabricated using EBL, metal evaporation and lift-off.

5.6.1 Design considerations for 2450 MHz SAW strain sensor

The most important constraint for this design is the lack of space. The mechanical parts used have an area with a flat surface of approx. 3 mm by 10 mm. This is the only area suitable for the considered lithography techniques. Optical lithography is currently only possible on flat samples (such as wafers) and EBL has a limited depth-of field in the μm range.

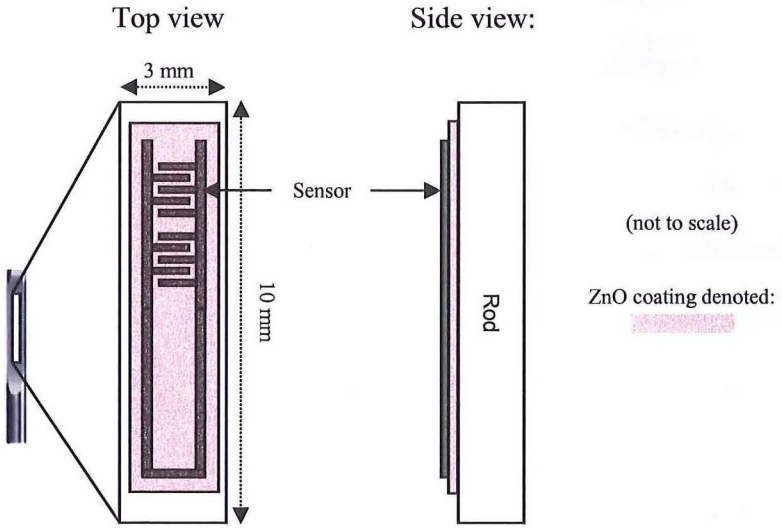

Figure 49: SAW structure on flat portion of stainless steel rod.

Figure 49 shows a schematic arrangement of the SAW structure consisting of SAW IDT, reflector and antenna loop. The insulating ZnO coating is located between the SAW structure and the rod. The SAW device consists of the SAW structure as described plus the ZnO sputter coated rod as substrate.
For detailed design considerations refer to section 1.1.

Table 11: Design of 2450 MHz SAW device.

Substrate material	Sputtered ZnO, thickness ≈ 500 nm
Metal for IDTs	Aluminium
Phase velocity of sound, v_s	ZnO: 9180 m/s (surface acoustic wave) [57]
Dielectric constant ZnO	10 … 37 [57], will need to be confirmed.
Center frequency, f_{RES}	2450 MHz
Theoretical acoustic wavelength, λ	3.75 μm $(\lambda = \frac{v_s}{f_{RES}})$
Chosen acoustic wavelength, λ	4 μm
Number of interdigital fingers, n	n = 50 (design rule)
Metallisation thickness, h	≈ 50 nm

In the literature, different values for the phase velocity have been reported [57, 58]. This might be caused by variation of the thickness of the sputtered ZnO and the type of base substrate. After fabrication of the first prototype the values of Table 11 will need to be confirmed. (Note: The following trials were done before the trials on the Si wafers (section 5.5) hence the value for the phase velocity as of [57] was taken.)

Antenna design

As simple antenna design, a modified $\frac{\lambda}{4}$ dipole as of Figure 49 has been considered.

As mentioned the rod is made of metal and therefore conductive. It will act as (floating) ground plane, effectively forming a capacitance between metal and the SAW structure. Therefore, the sputtered ZnO will act as a dielectric substrate backed by a ground plane. Any dielectric substrate with properties other than air/vacuum will change the characteristics of the antenna structure [63].

The mechanical length l_ε of the antenna is influenced by the constant of the dielectric material (ZnO) as follows: $l_\varepsilon = \frac{l_o}{\sqrt{\varepsilon}}$

where ε is the relative dielectric constant of ZnO and l_0 is the length of the antenna structure with air/vacuum as dielectricum

A $\frac{\lambda}{4}$ antenna radial with air as dielectricum has a length of around 3 cm (working in 2450 MHz).

Assuming a relative dielectric constant of 10, the antenna length would be roughly 1/3 of the original size and therefore around 1 cm. It should be feasible to get an effective working antenna on the area provided. More design guidelines in regards to small scale antenna design and antenna matching can be found in [64, 65].

Because of all these non-quantified influences it was decided to build a series of prototypes and test the influence of various parameters on the fabricated device performance.

5.6.2 Fabrication sequence

The SAW structure was fabricated on a rod as follows (refer to Figure 10 and Figure 11 for more details):

- Polishing of rod using polishing paste and fine sandpaper
- Cleaning of rod
- Sputter coating of ZnO (refer to section 2.10.2)
- Spinning of bilayer PMMA with curing
- Exposure using Raith 150 EBL
- Developing using 1:3 MIBK:IPA
- Al evaporation (100 nm) using thermal evaporation
- Lift-off in acetone

Outcome:

- SAW structure inclusive antenna is well defined.
- ZnO acts as insulating layer, very high resistance (same as glass) measured between conductive layer and rod (prerequisite for working device).
- The measured resistance of the antenna structure is too high (measured > 300 Ω across antenna loop). This means the antenna is very lossy and ineffective. The Al (conductive layer) is very thin (100 nm). Note surface roughness of evaporated Al in Figure 51 and Figure 52.

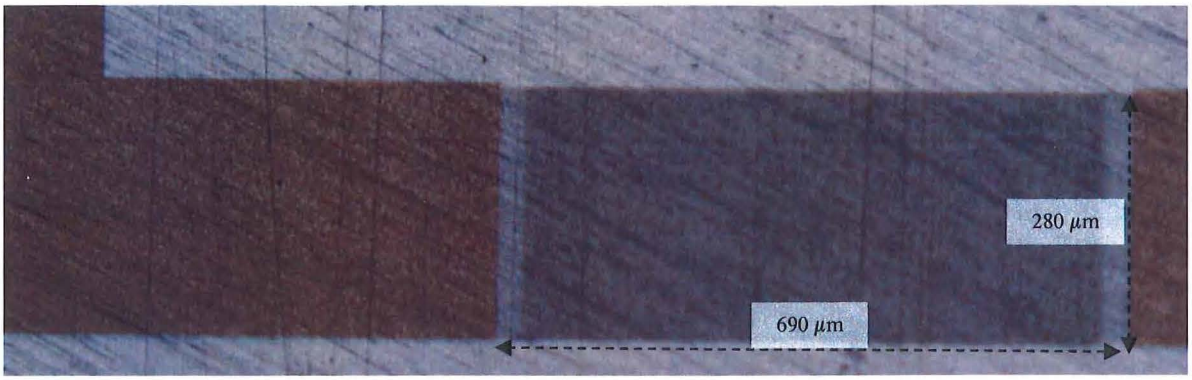

Figure 50: Optical microscope image of detail of SAW structure on rod (top view).

Figure 50 shows a part of the antenna and the connection with the IDT. The streaks which are clearly visible are caused by the polishing.

Figure 51: Optical microscope image of IDT (top view, close-up).

In Figure 51 the contacts of the IDT are shown, with a line width of 1 μm. A rough surface is evident which leads to high ohmic losses of the Al coating.

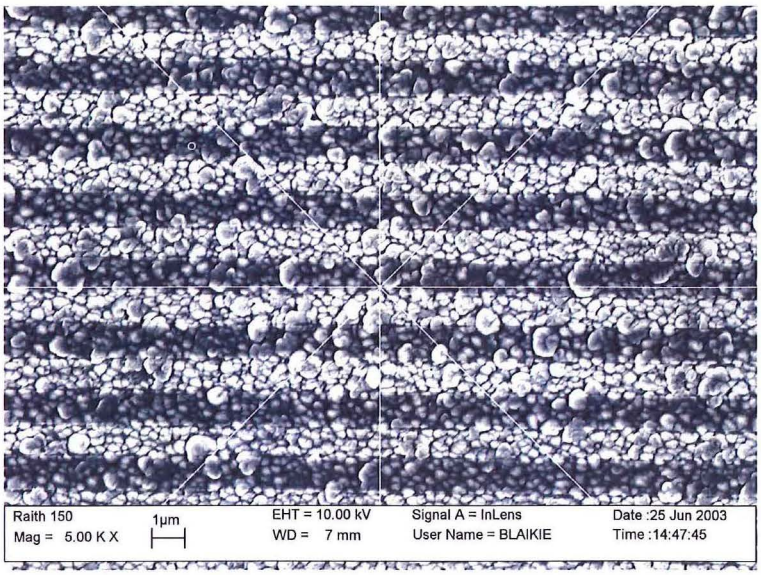

Figure 52: SEM image showing IDT (top view).

Figure 52 was taken with the Raith 150 SEM and shows more detailed surface roughness. The grain size of the sputtered ZnO appears in the range of 100 nm to 1 μm. The bright coloured strips are covered with 100 nm of evaporated Al and the dark coloured strips are bare sputtered ZnO. It appears that the Al does not entirely cover the area, but it sits merely on the tops of the sputtered grains.

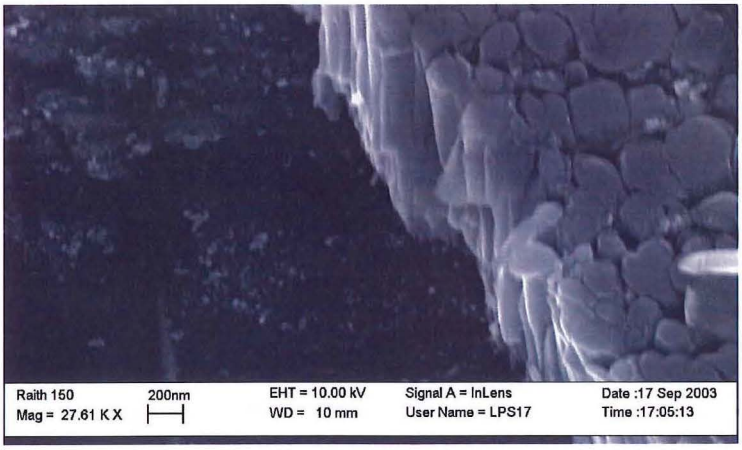

Figure 53: SEM image showing sputtered ZnO on rod (view from angle).

In Figure 53 the polycrystalline crystal growth on the rod is easily visible. It appears that the crystals have a well defined and flat upper phase (where the growth stopped).

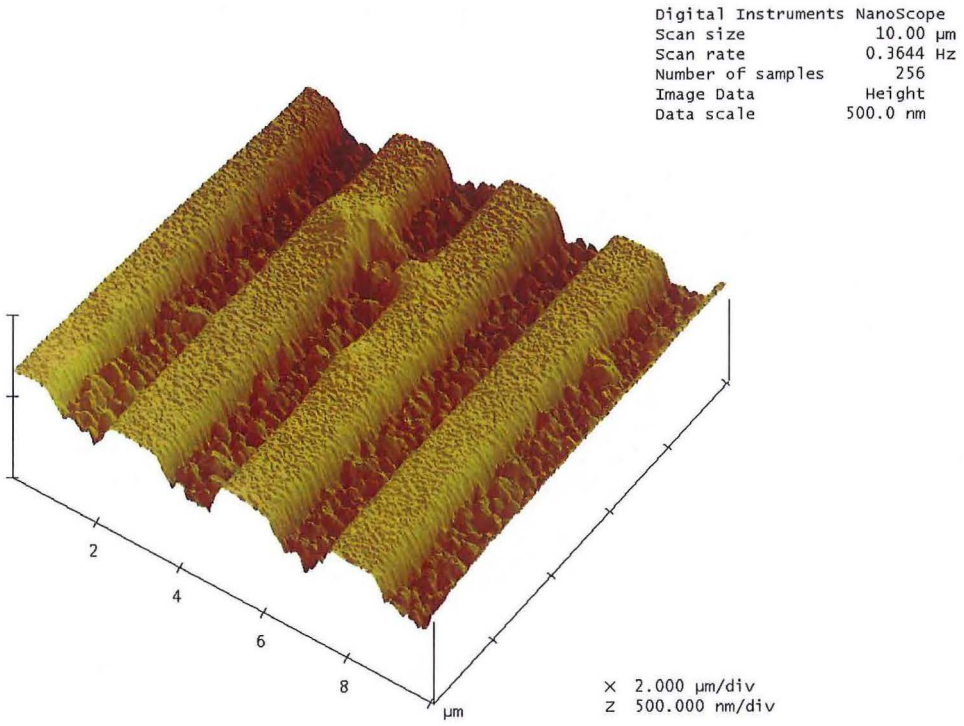

Figure 54: AFM scan in tapping mode shows details of SAW device.

Figure 54 shows sputtered ZnO on the trenches and evaporated Al on the ridges. This picture is taken off the same sample as shown in Figure 53. The rough surface of the ZnO is clearly visible. The Al coated IDTs look much smoother than on SEM images but this might be an effect of the limits with AFM imaging (as mentioned in Section 3.1.5). Also, the trenches appear narrower than they are in reality (due to resolution limits of AFM imaging [48]).

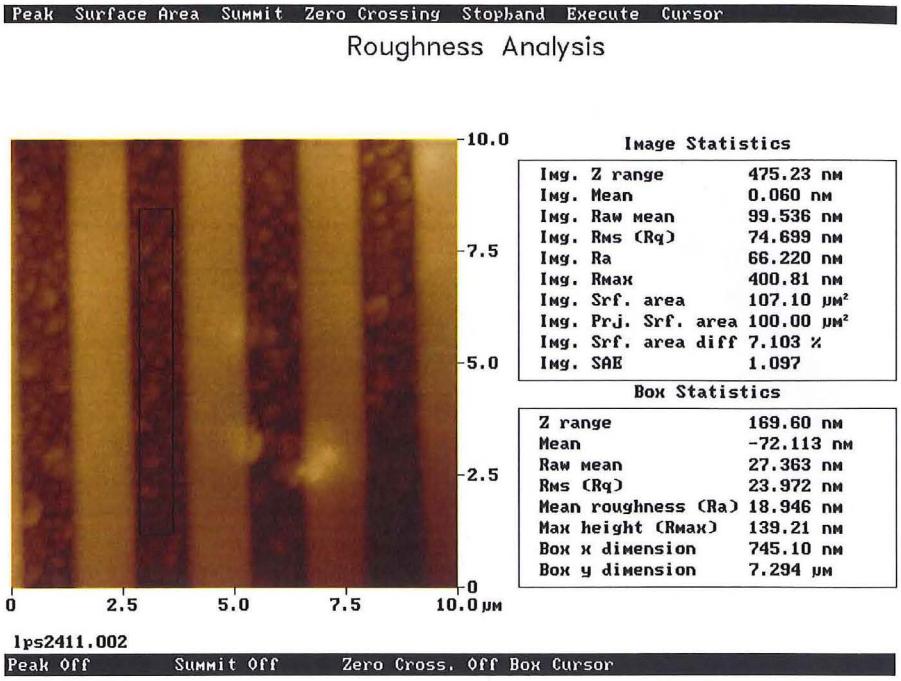

Figure 55: Roughness analysis off AFM scan for sputtered ZnO.

(See figure below for comments.)

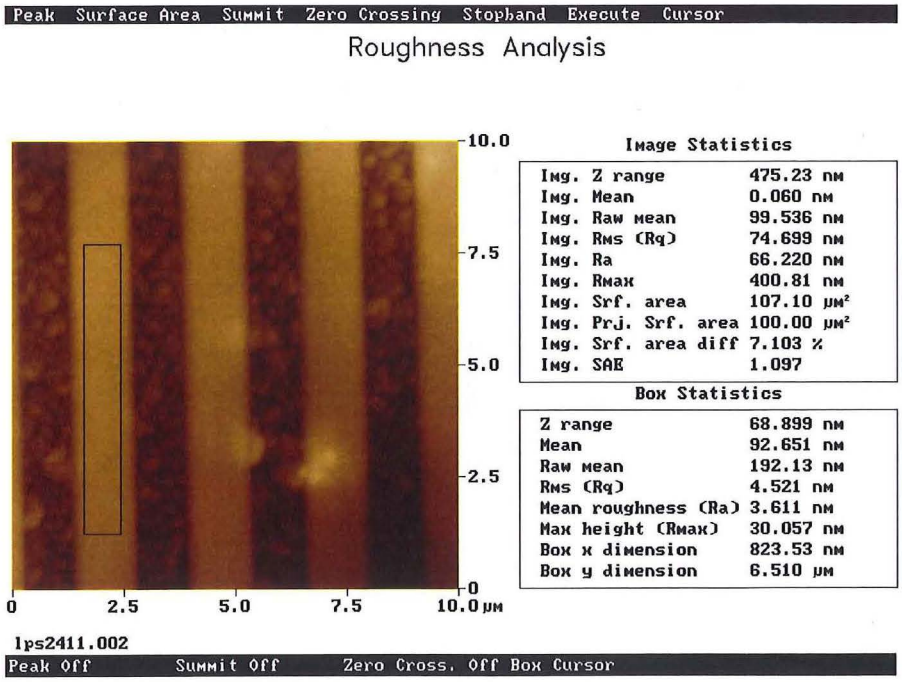

Figure 56: Roughness analysis off AFM scan for evaporated Al on sputtered ZnO.

Figure 55 and Figure 56 show roughness values of both the sputtered ZnO and the Al tracks which are evaporated on top. The mean roughness (Ra) is around 24 nm for sputtered ZnO and around 3.6 nm for

evaporated Al respectively. It has to be noted that this figure is the average over a very small areas only and does not give an indication for the whole area used for the SAW device.

5.6.3 Trials with thicker Al coating

Additional trials were done with thicker Al (220 nm), in an attempt to improve the conductivity. The bilayer of PMMA has a thickness of only 200 nm. Therefore, lift-off was very hard and only partially successful.

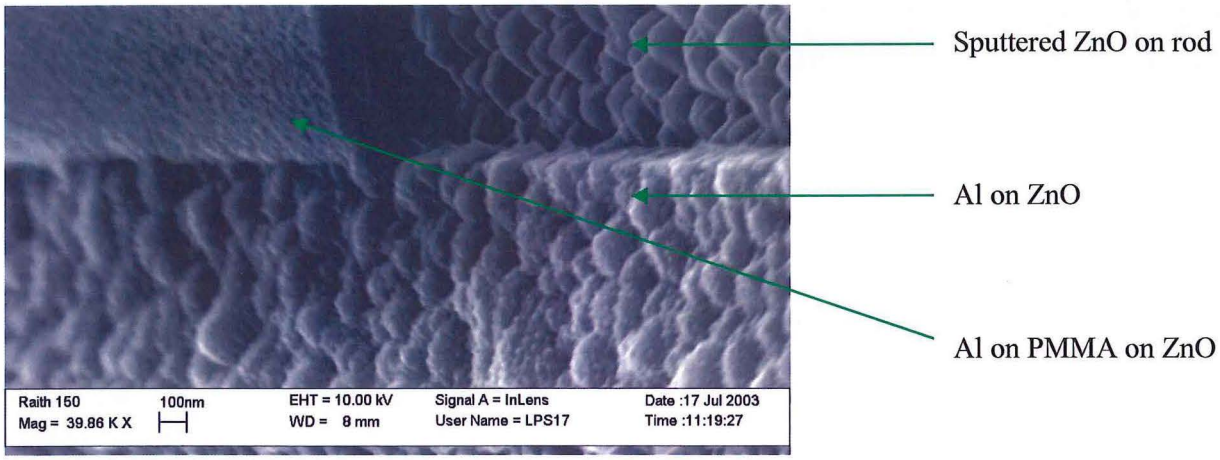

Figure 57: SEM image of partial lift-off.

Figure 57 shows some interesting details: Al on ZnO appears with the same surface roughness as the ZnO. But Al on PMMA looks much smoother. PMMA seems to have a smoothing effect.

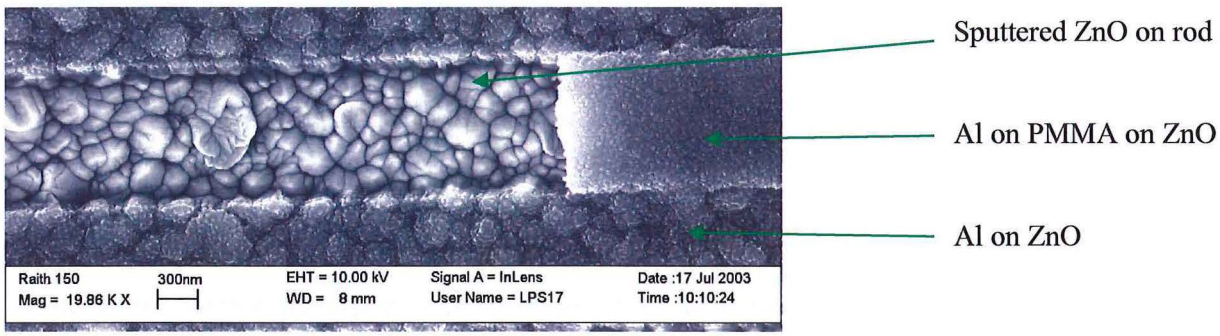

Figure 58: SEM image of partial lift-off.

Figure 58 shows another close-up image. The individual ZnO crystals and the surface roughness are clearly visible. The two Al strips appear semi-opaque and the structure of the ZnO can be seen. Again, it appears that the Al on top of the PMMA is much smoother.

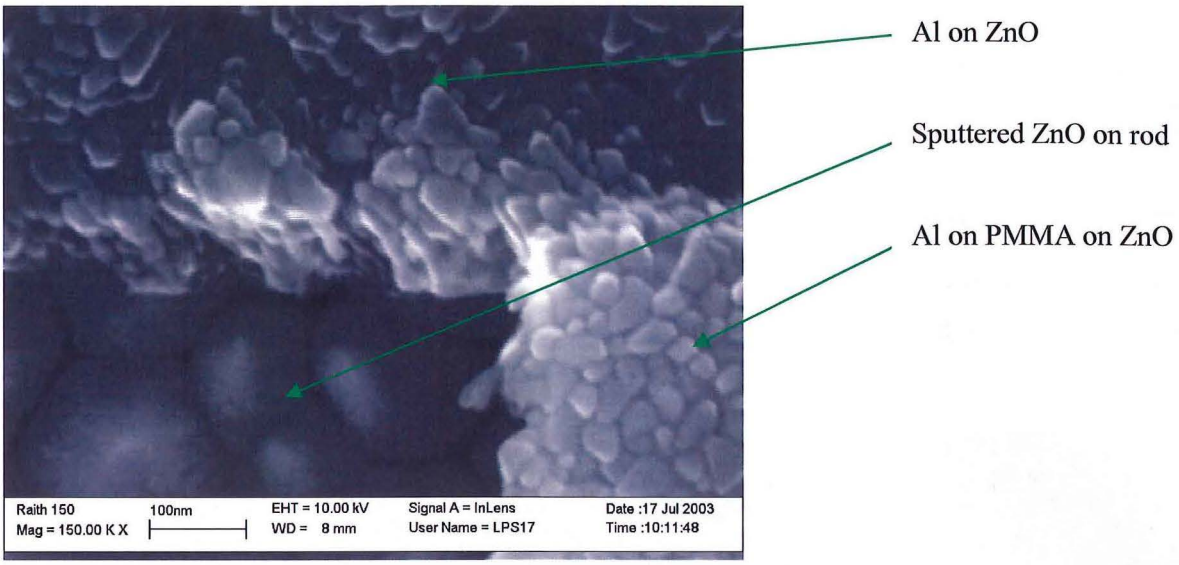

Figure 59: SEM image of rod with partial lift-off.

Figure 59 reveals that the Al is actually deposited as small grains and again the surface is much smoother where the Al is deposited on top of PMMA. (Due to the shape of this sample no AFM image could be taken.)

5.6.4 Trial with smoothing layer

As shown in Figure 58 and Figure 59, PMMA smoothes out the rough surface of the sputtered ZnO. The implication is, that PMMA is soluble in acetone and will be dissolved during development. In order to avoid this, PMMA was spun on the small flat area only (area not to be covered was masked off), whereas ZnO was sputtered across the whole sample, which should insulate the PMMA from acetone contact. A trial was run as follows:

- A single layer of LMW PMMA (4%), was spun on polished rod and pre-baked
- 500 nm of ZnO was sputtered on the whole rod (including the PMMA)

After this, the sample was soaked in acetone. Unfortunately, the ZnO lifted off very quickly. PMMA is therefore not suitable as a smoothing layer, as it will be dissolved by subsequent processes, even after sputtering of ZnO. A suitable smoothing layer will need to be identified at a later stage.

5.7 Summary

The sputtering of ZnO was optimised and the quality of the sputtered coatings analysed. ZnO was sputtered on Si wavers and SAW devices were fabricated using optical lithography and the devices were

successfully tested. Following these preliminary trials, a SAW device with integrated antenna was designed to fit on the rod and to be fabricated using EBL. Several prototypes were fabricated but lift-off was tricky. The surface roughness of the rods seems unsuitable as a base for a SAW device.

Another problem recognised is the spinning of PMMA on rods. The commonly used spinners are designed for flat samples (wafers). In order to spin PMMA onto the rod, the rod was fixed temporarily in a sample holder by using sticky tape. The rod as such has only one flat surface and due to its shape will cause lots of disturbance in the airflow thus leading to uneven spreading of the PMMA. The solution might be using a special holder or dip coating.

Chapter 6

Conclusions and outlook

SAW devices have been successfully designed, fabricated and tested on Lithium Niobate substrate. $LiNbO_3$ has unique piezoelectric but also pyroelectric properties. SAW oscillators and ID tags have been designed using L-Edit with 180 MHz working frequency, which resulted in feature sizes of 5 μm. They were fabricated using optical lithography, metal evaporation and wet etching. Testing using a network analyser showed a wireless range of up to 2.5 metres. The 360 MHz SAW devices were fabricated using the same methods which lead to a feature size of 2.5 μm and the wireless range was in the same range.

More SAW devices were designed using L-Edit with a working frequency of 2450 MHz. The resulting feature size of around 350 nm required fabrication using Electron Beam Lithography. During the fabrication of SAW devices on $LiNbO_3$ charging issues became evident, which made a successful fabrication impossible. Three procedures were identified and trialled to overcome this issue. The first one was using a conductive polymer: After coating with PMMA, the wafer was coated with a conductive polymer (PEDOT/PSS). This layer somewhat improved the conductivity but the results were still unsatisfactorily. The second attempt using 10 nm of gold as a conductive layer lead to good exposures, but the alignment before EBL was not possible due to insufficient contrast. The third and most successful attempt to overcome the charging problems was with a technique which chemically reduces the wafer surface through oxidation. With this method, the wafer is brought up to around 600 °C in a furnace in 5% H_2/95% N_2 atmosphere which oxidises the surface. This makes the material less susceptible to pyroelectric charging. SAW IDTs were finally fabricated on a reduced wafer using Electron Beam lithography, metal evaporation and lift-off but were unsuccessful due to malfunctions of the pattern generator which lead to missing features and imperfect exposures.

In order to get SAW devices working on irregularly shaped samples, a way had to be found to add a piezoelectric layer to the samples of interest. Zinc Oxide is not only a versatile material with advantageous piezoelectric properties but it can be coated on a wide range of materials using sputtering.

ZnO has been sputtered both on planar Si samples and irregularly shaped rods. The sputtered ZnO samples have been characterised using various methods: Rutherford backscattering showed good stoichiometry, X-ray diffraction confirmed [002] growth of ZnO, the coatings have high resistance, SEM imaging showed strong directional growth of the individual crystals, and AFM imaging was used to assess the mean surface roughness (Rms), which was around 24 nm for sputtered ZnO and around 3.6 nm

for evaporated Al. On the planar sample, a SAW device was fabricated using optical lithography and successfully tested.

On the rod, a bilayer of PMMA was spun and a SAW device including antenna was fabricated using electron beam lithography, metal evaporation and lift-off. However, due to the rough surface of the sample the lift-off was only partial and no device could be tested.

Outlook

Besides successful fabrication of SAW devices on $LiNbO_3$ we have proven that sputtered ZnO is a suitable piezoelectric material with high performance for SAW applications. Normally, a smooth surface (i.e. polished wafer) is a base material for successful lithographical steps. With our "real world" application and less than perfect substrate (rods, which are mechanical parts of machines and subject to wear and tear), problems have become evident which have created considerable obstacles. The recently acquired sputtering system will enable further exploration. Simple surface preparation, such as using a primer layer to smooth out small scratches will need to be established. Another approach is the use of thicker photo resist for EBL which would enable lift-off of thicker metal coatings.

The sensitivity of fabricated SAW strain sensors will need to be characterised and ways to increase the range and engineer the sensitivity will need to be found.

The existence of interface acoustic waves (IAW) will have to be verified. IAW might be propagating along the interface between the sputtered ZnO and the rod, possibly with a different phase velocity than the SAW wave.

In the semiconductor industry, the trend towards further miniaturisation is a main driving force and a small footprint of any component is critical. Therefore the determination of limits for minimal size and maximal frequency for SAW devices should be investigated. It is envisaged that the highest possible operation frequency will be constrained not only by the lithographical technique (Electron Beam lithography/ENFOL) but also by the grain size/roughness of the substrate. The University of Canterbury Electrical Engineering department's state-of-the-art Raith 150 EBL system has the potential to define small features down to 20 nm.

On the application side, further applications beyond measuring strain only should be investigated. It should be possible to complement the SAW structure with on-board intelligence, such as an Application Specific Integrated Circuit (ASIC), which would enable the structure to "react" to changing measured values. It would be feasible to set up a structure in such a way that it would send out a signal only if certain conditions were met (i.e. alarm condition).

Various nanofabrication techniques, like EBL for prototyping but also emerging techniques such as Nanoimprint, could be investigated. The latter might hold the key for cheap mass-production, which is critical for market acceptance.

Interrogation of single SAW devices using a network analyser has been successfully demonstrated. A requirement for commercial use is the ability to interrogate several SAW sensors concurrently in a multi sensor environment. Currently another student is building a dedicated interrogator.

Chapter 7

Publications

Schuler, L.P., Alkaisi, M. M., Meade, W. J., *Wireless switching based on passive surface acoustic wave devices (confidential report)*. 2003, Canesis Network Limited: Lincoln.

Schuler, L.P., Alkaisi, M. M., *Wireless Force-Sensing in Bone Implants (poster presentation)*. 2003, FiRST Scholarship Awards: Christchurch.

Schuler, L.P., Alkaisi, M. M., Meade, W. J., *Wireless identification based on passive surface acoustic wave devices. (confidential report)*. 2003, Canesis Network Limited: Lincoln.

Bibliography

1. Ruppel, C.C.W., L. Reindl, and R. Weigel, *SAW devices and their wireless communications applications.* IEEE Microwave Magazine, 2002. 3(2): p. 65-71.
2. Ruppel, C.C.W., Fjeldly, Tor A., *Advances in surface acoustic wave technology, systems and applications.* Selected Topics in Electronics and Systems. Vol. 19. 2000. 324.
3. Campbell, C.K., *An Overview of SAW Devices For Mobile/Wireless Communications*, in *Understanding Surface Acoustic Wave (SAW) Devices for Mobile and Wireless Applications and Design Techniques.* 2003.
4. Crystal Technology, I., *Lithium Niobate surface acoustic wave wafer.* 1999.
5. Nguyen, C.T.-C. *Microelectromechanical devices for wireless communications.* in *Proceedings of the 1998 IEEE 11th Annual International Workshop on Micro Electro Mechanical Systems, Jan 25-29 1998.* 1998. Heidelberg, Ger: IEEE, Piscataway, NJ, USA.
6. Wright, P.V., *A review of SAW resonator filter technology.* Ultrasonics symposium, 1992. 1992: p. 29-38.
7. Rayleigh, L., *On Waves Propagated Along The Plane Surface Of An Elastic Solid.* Proc Lond Math Soc, 1885. (17):4-11.
8. Schuler, L.P., Alkaisi, M. M., Meade, W. J., *Wireless identification based on passive surface acoustic wave devices.* 2003, Canesis Network Limited: Lincoln. p. 10.
9. Schuler, L.P., Alkaisi, M. M., Meade, W. J., *Wireless switching based on passive surface acoustic wave devices.* 2003, Canesis Network Limited: Lincoln. p. 10.
10. Ash, D.L., *SAW-based hybrid transceivers in slam packaging with frequency range from 200 to 1000 MHz.* Proceedings of the 1998 International Ultrasonics Symposium, Oct 5-Oct 8 1998, 1998. 1: p. 389-398.
11. Kurosawa, M., M. Takahashi, and T. Higuchi, *Friction drive surface acoustic wave motor.* Ultrasonics, 1996. 34(2-5): p. 243-246.
12. Kurosawa, M., M. Takahashi, and T. Higuchi, *Ultrasonic linear motor using surface acoustic waves.* IEEE Transactions on Ultrasonics, Ferroelectrics, and Frequency Control, 1996. 43(5): p. 901-906.
13. Collings, A.A.F. and A.F. Caruso, *Biosensors: recent advances.* 1997.
14. Schimetta, G., et al. *Wireless pressure and temperature measurement using a SAW hybrid sensor.* in *2000 IEEE Ultasonics Symposium, Oct 22-25 2000.* 2000. San Juan: Institute of Electrical and Electronics Engineers Inc.
15. Jain, M.K., Q. Cai, and C.A. Grimes, *A wireless micro-sensor for simultaneous measurement of pH, temperature, and pressure.* Smart Materials and Structures, 2001. 10(2): p. 347-353.
16. Lazzaroni, M., et al. *Remote measurement and monitoring of critical washing process data directly inside the washing machine drum.* in *IMTC/2000 - 17th IEEE Instrumentation and Measurement Technology Conference 'Smart Connectivity: Integrating Measurement and Control', May 1-May 4 2000.* 2000. Baltimore, MD, USA: Institute of Electrical and Electronics Engineers Inc., Piscataway, NJ, USA.
17. Schuler, L.P., Alkaisi, M. M., *Wireless Force-Sensing in Bone Implants.* 2003: 2003 FiRST Scholarship Awards, Christchurch.
18. White, R.M. and F.W. Voltmer, *Direct Piezoelectric Coupling to Surface Elastic Waves.* Appl. Phys. Lett., 7, pp. 314-316, 1965.
19. Yamanouchi, K. *GHz-range saw device using nano-meter electrode fabrication technology.* in *Proceedings of the 1994 IEEE Ultrasonics Symposium. Part 1 (of 3), Nov 1-4 1994.* 1994. Cannes, Fr: IEEE, Piscataway, NJ, USA.
20. Yamanouchi, K., et al., *10 GHz surface acoustic wave filters with narrow-gap interdigital transducer structure.* Japanese Journal of Applied Physics, Part 1: Regular Papers & Short Notes & Review Papers. Proceedings of the 1995 16th Symposium on Ultrasonic Electronics, USE95, Nov 27-29 1995, 1996. 35(5B): p. 2994-2996.

21. Hachigo, A., et al. *10GHz narrow band SAW filters using diamond.* in *1999 IEEE Ultrasonics Symposium, Oct 17-Oct 20 1999.* 1999. Caesars Tahoe, NV, USA: Institute of Electrical and Electronics Engineers Inc., Piscataway, NJ, USA.
22. Kuribayashi, M. and T. Higuchi. *Surface acoustic wave linear motor.* 1999.
23. Russell, D., *Longitudinal and Transverse Wave Motion, http://www.gmi.edu/~drussell/Demos/waves/wavemotion.html.* 1999.
24. Briot, J.B., et al. *An accurate design and modeling tool for the design of RF SAW filters.* in *2001 Ultrasonics Symposium, Oct 6-10 2001.* 2001. Atlanta, GA: Institute of Electrical and Electronics Engineers Inc.
25. Hashimoto, K., T. Omori, and M. Yamaguchi, *Analysis of SAW excitation and propagation under periodic metallic grating structures.* International Journal of High Speed Electronics and Systems., 2000. Vol. 10(No 3).
26. Emanetoglu, N.W., *High frequency surface acoustic wave filters using epitaxial ZnO thin films grown on sapphire substrates*, in *Graduate Scholle - New Brunswick.* 1998, The State University of New Jersey: Rudgers. p. 60.
27. McCollister, M.J. and S.M. Richie. *An efficient algorithmic approach to the design of SAW coupled resonator filters for design automation.* in *2000 IEEE Ultasonics Symposium, Oct 22-25 2000.* 2000. San Juan: Institute of Electrical and Electronics Engineers Inc.
28. Photox, *Lithium Niobate Crystal.* 2000.
29. Auret F D, G.S.A., Hayes M, Legodi M J, van Laarhoven H A and Look D C, *Electrical characterization of 1.8 MeV proton-bombarded ZnO.* Appl. Phys. Lett. 79 3074-6, 2001.
30. Yang, J., P.U. Voigt, and R. Koch, *Nanoscale investigation of longitudinal surface acoustic waves.* Applied Physics Letters, 2003. 82(12): p. 1866-1868.
31. Water, W. and S.-Y. Chu, *Physical and structural properties of ZnO sputtered films.* Materials Letters, 2002. 55(1-2): p. 67-72.
32. Ng, H.T., B. Chen, and J. Li, *Optical properties of single-crystalline ZnO nanowires on m-sapphire.* Applied Physics Letters [H.W. Wilson - AST], 2003. 82(13): p. 2023.
33. Banerjee, D., et al., *Large-quantity free-standing ZnO nanowires.* Applied Physics Letters, 2003. 83(10): p. 2061-2063.
34. Geng, B.Y., et al., *Synthesis and optical properties of S-doped ZnO nanowires.* Applied Physics Letters, 2003. 82(26): p. 4791-4793.
35. Heo, Y.W., et al., *Site-specific growth of ZnO nanorods using catalysis-driven molecular-beam epitaxy.* Applied Physics Letters, 2002. 81(16): p. 3046.
36. Kim, S.-W., S. Fujita, and S. Fujita, *Self-organized ZnO quantum dots on SiO2/Si substrates by metalorganic chemical vapor deposition.* Applied Physics Letters, 2002. 81(26): p. 5036-5038.
37. Rai-Choudhury, P., *Handbook of microlithography, micromachining, and microfabrication.* 1997. Volume 1: Microlithography (SPIE PRESS Monograph Vol. PM39).
38. Tanner Research, I., *http://www.tanner.com/.*
39. MicroChem, *Nano PMMA and Copolymer. Useful introduction about PMMA.* 2002.
40. Gale, B.K., *Wet Etching and Bulk Micromachining. Fundamentals of Micromachining.* 2002.
41. Standifer, E.M., Jundt, D. H., Norwood,R. G., Bordui, P. F. *Chemically Reduced Lithium Niobate Single Crystals: Processing, Properties and Improvements in SAW Device Fabrication and Performance.* in *Reprinted from IEEE Proceedings of the 1998 International Frequency Control Symposium.* 1998: IEEE.
42. Thornton, J.A., *The microstructure of sputter-deposited coatings.* 1986.
43. Vellekoop, M.J., et al., *Compatibility of zinc oxide with silicon IC processing.* Sensors and Actuators, A: Physical Transducers '89: Proceedings of the 5th international Conference on Solid-State Sensors and Actuators and Eurosensors III. Part 4, Jun 25-30 1989, 1990. 23(1-3): p. 1027-1030.
44. Southin, J.E.A., et al., *e31,f determination for PZT films using a conventional 'd33' meter.* Journal of Physics D: Applied Physics, 2001. 34(10): p. 1456-1460.
45. Kholkin, A.L., et al., *Interferometric measurements of electric field-induced displacements in piezoelectric thin films.* Review of Scientific Instruments, 1996. 67(5): p. 1935.

46. Kessler, P., G. Soelkner, and K.C. Wagner. *Imaging of the wave field of surface acoustic wave devices.* in *IEEE Ultrasonic Symposium.* 1991.
47. von Preissig, F.J., H. Zeng, and E.S. Kim, *Measurement of piezoelectric strength of ZnO thin films for MEMS applications.* Smart Materials and Structures, 1998. 7(3): p. 396-403.
48. Instruments, D., *Scanning probe microscopy training notebook.*
49. Passian, A., et al., *Piezoresistive detection of acoustic waves.* Review of Scientific Instruments, 2003. 74(2): p. 1031-1035.
50. Malovichko, G., Grachew, V., *Evolutions of conception of intrinsic and extrinsic defects in lithium niobate.* 1998-2001, University of Osnabrueck, Germany.
51. Alkaisi M.M, et al., *Sub-diffraction-limited pattering using Evanescent near field optical lithography.* Applied Physics Letters, 1999. 75(22): p. 5360.
52. McNab S.J, Blaikie R.J, and Alkaisi M.M, *Analytical study of gratings patterned by evanescent near field optical lithography.* Journal of Vacuum Science and Technology B, 2000. 18(6)(2900 Nov /Dec).
53. Alkaisi M.M, Blaikie R.J, and M. S.J, *70 nm features on 140 nm period using evanescent near field optical lithography.* Microelectronic Engineering, 2000. 53(237).
54. Alkaisi M.M, Blaikie R.J, and M. S.J, *Nanolithography in the evanescent near field.* Advanced Materials, Special issue on material science in Australia and New Zealand,, 2001. 13(877).
55. Alkaisi M.M, Blaikie R.J, and McNab S.J, *Low temperature nanoimprint lithography using silicon nitride molds.* Microelectronic Engineering, 2001. 57-58(367).
56. Alkaisi M.M, Jayatissa W, and K. M, *Multilevel nanoimprint lithography.* Current applied Physics, Elsevier Science, 2004.
57. Choi, K.H., et al. *Effect of dielectric layer in ZnO/dielectric/Si layered structure on GSAW and HVPSAW propagation properties.* in *2000 IEEE Ultasonics Symposium, Oct 22-25 2000.* 2000. San Juan: Institute of Electrical and Electronics Engineers Inc.
58. Didenko, I.S., F.S. Hickernell, and N.F. Naumenko, *Experimental and theoretical characterization of the SAW propagation properties for zinc oxide films on silicon carbide.* IEEE Transactions on Ultrasonics, Ferroelectrics, and Frequency Control, 2000. 47(1): p. 179-187.
59. Kitabayashi, H. and P.M. Smith, *Analysis of SAW propagation in gratings on ZnO/diamond substrates.* IEEE Transactions on Ultrasonics, Ferroelectrics, and Frequency Control, 2001. 48(1): p. 249-261.
60. Kitabayashi, H. and P.M. Smith. *Dispersion properties of ZnO/Diamond layered structures under periodic metal gratings.* in *Ultrasonics Symposium, 1999. Proceedings. 1999 IEEE.* 1999.
61. Clatot, S., V. Laude, and e. al. *Sensitivity of interface acoustic waves to the nature of the interface.* in *2003 IEEE ultrasonics symposium.* 2003.
62. Muller, C., *Sputtered Zinc Oxide And Lead Zirconate Titanate Piezoelectric Thin Films On Optical Fibres.* 2000, EPFL: Lausanne.
63. Codreanu, I. and G.D. Boreman, *Influence of dielectric substrate on the responsivity of microstrip dipole-antenna-coupled infrared microbolometers.* Applied Optics, 2002. 41(10): p. 1835-1840.
64. Smith, K., *Antennas for low power applicaitons.* RF Monolithics, Inc., 2000.
65. RFM, *ASH transceiver antenna impedance matching.* RF Monolithics, Inc., 2001.